Results in Engineering 30 (2026) 110908

Contents lists available at ScienceDirect

Results in Engineering

journal homepage: www.sciencedirect.com/journal/results-in-engineering

Research paper

Oil flows inside a single-stage jet-lubricated mechanical transmission with spur gears

Luca Bonaiti [a,*], Lorenzo Valsecchi [a], Paolo Pisani [b], Lorenzo Maccioni [c], Franco Concli [c], Javier Sanchez-Espiga [d], Carlo Gorla [a], Sergio Sartori [b]

[a] Dipartimento di Meccanica, Politecnico di Milano, Via La Masa, 1, Milano (MI), Italy
[b] Helicopter Division, Leonardo S.p.A, Via Giovanni Agusta, 520, Cascina Costa di Samarate (VA), Italy
[c] Faculty of Engineering, Free University of Bozen-Bolzano, Via Buozzi 1, Buozzistraße 1, Bolzano (BZ), Italy
[d] Department of Structural and Mechanical Engineering, ETSIIT University of Cantabria, Avda. de los Castros s/n 39005, Santander, Spain

ARTICLE INFO

Keywords:
Gearboxes
Jet lubrication
Experimental analysis
Oil flows

ABSTRACT

Besides ensuring physical separation between contact surfaces and removing the heat, lubrication oil in helicopter (MGB)s is also used to convey any metallic debris to instrumentation capable of providing indications on the health status of the MGB itself. Accurate knowledge of the actual oil flow patterns, not only of its main directions, and of the parameters that may influence them is required for this mechanism to function properly. A new test rig is proposed here, designed to provide insight of the oil flows inside a jet-lubricated test gearbox with a quantitative approach rather than a qualitative one. An extensive test campaign has been conducted on this test rig, and the results are reported here. Subsequently, these results are discussed to highlight the factors that most influence the behaviour of the lubricant oil flow after the jet impingement on the flanks.

1. Introduction

Gears are machine elements that transmit power (i.e., rotation and torque) between different axes, modifying the torque/speed relationship with an adequate level of efficiency and compactness. Their operation principle relies on a loaded contact in which rolling and sliding occur simultaneously along the meshing flanks. In common engineering practice, lubrication is introduced to maintain a fluid film between the contacting surfaces, hence keeping them separate, and to remove the heat produced during meshing. Oil is selected for high-speed transmissions [1]. Oil can be supplied to the gear flanks with two different strategies: splash lubrication, in which rotating gears enter the oil sump, and jet lubrication, where oil is supplied through dedicated nozzles. This latter lubrication strategy, which is the focus of this article, is adopted because of it great advantages on the overall gearbox efficiency.

Helicopter MGBs are particularly critical due to the potential catastrophic consequences of their failure. For this reasons, their lubrication, in addition to preventing failures, has a third function, related to system safety: it allow for the detectability of potential component damage. Indeed, inside MGBs, the oil collects potential metallic debris resulting from component damage and transport it to a chip detector, which provides information on the health status. Here, the designer must ensure that the lubrication oil is supplied to the critical areas, where it collects the possible debris and then it provides such debris to the chip detector. The latter should be placed in a position favourable to the oil collection. Hence, it must be ensured "*that the chip detection systems that are installed in rotorcraft rotor drive systems achieve an acceptable minimum level of effectiveness in detecting the incipient degradation or failure of components of the rotor drive system*", as stated by (EASA) in 2021 [2]. Therefore, it is fundamental the knowledge of oil flows direction, together with their magnitude, as well as the factors that govern them. All of the above must be done without focusing only on the meshing region, but also after the jets impingements on the flaks while looking to the whole housing.

To illustrate the scale of a typical MGB, the AW189 MGB incorporates two input shafts, each driven by a ≈ 1.5 MW turbine rotating at approximately 21 000 rpm, and delivers power to the main rotor at roughly 290 rpm. This configuration yields an overall speed reduction of about 75:1 and with a total input power of almost 3 MW. The lubrication system employs almost 30 L of oil to service all critical elements, including gears and bearings, through a combination of dip-based splash lubrication and jet lubrication [3,4].

This context have strengthened the industrial interest in using (CFD) tools during design stages to characterise internal lubrication flows. In particular, the need to enhance the detectability of metallic debris [2] has intensified the efforts to predict how oil circulates within complex gearbox architectures. Recent studies have demonstrated that CFD

* Corresponding author.
E-mail address: luca.bonaiti@polimi.it (L. Bonaiti).

https://doi.org/10.1016/j.rineng.2026.110908
Received 28 February 2026; Received in revised form 15 April 2026; Accepted 5 May 2026
Available online 8 May 2026

simulations can provide a reliable description of lubrication mechanisms in geared transmissions (e.g., [5–9]). Regardless of the modelling approach, it is good engineering practice to validate numerical predictions with experimental evidence. Such validation may involve tests on the complete component, on a representative subsystem, on a simplified configuration, or, when no other option is available, on data extracted from the literature. For splash-lubricated systems, numerous studies provide reference measurements suitable for benchmarking. By contrast, comparable datasets for jet-lubricated configurations remain scarce, limiting the availability of directly applicable validation material, as discussed in [10] and in Section 2.

The work presented here is indeed part of a broader project aimed at the CFD simulation of the lubrication flows within an MGB. Since validation at the level of the complete system is complex, and in view of the limited experimental data currently available, the validation activity was carried out on a dedicated, simpler, measurable system. This choice required the development of a new dedicated test rig on which the necessary measurements can be performed. Whenever possible, the operating conditions were kept as close as possible to those of the real application, including, for instance, the oil type, the nozzle characteristic and the shrouding dimensions. Such test rig is the focus of this article.

After discussing the rationale behind the proposed test rif (see Section 2) and its design (see Section 3), the present study offers engineers and researchers a dedicated experimental dataset related to the oil distribution and its main flow paths in jet lubrication of meshing gear under different operating conditions. The database presented hereinafter is based on what can be considered the simplest and most straightforward quantity to measure: the amount of oil collected by pockets arranged radially around the gear pair. Despite its simplicity, this quantitative approach is rarely, if ever, adopted by the existing literature. The dataset proposed Section 4 is enriched with high-speed recordings of the gear meshing process.

The results of the tests presented in Section 5 are used to provide new insight on oil flows within a gearbox, moving from the classical approaches to a newer (and quantitative) one. This allow to investigate the relevant parameters involved in the oil flows by looking to the actual flows. In particular, here it is observed the influence of gear rotational speed, the activation of multiple nozzles, nozzle pressure (and thus flow rate), oil temperature (affecting both flow rate and lubricant properties) and variations in gear geometry on the resulting oil flows.

2. Background

The earliest studies on jet lubrication date back to the 1970s. First, considerable attention was devoted to the ability of the jet to penetrate the space between meshing teeth, so as to ensure adequate flank lubrication. This topic was investigated primarily by Townsend and Akin through both experimental and numerical approaches. This lead to of equations describing the jet behaviour under “in-mesh” conditions, where the jet is directed toward the engaging side of the mesh, and “out-of-mesh” conditions, where it is directed toward the disengaging side, as well as for jet velocities either lower or higher than the peripheral speed of the tooth (e.g., [11–14]). These studies also examined the ability of the jet to remove heat and the resulting effects on gear temperature (e.g., [15,16]). They also provided some of the first high-speed images of the phenomenon. Further investigations began evaluate the role of jet lubrication on the overall efficiency of the transmission (e.g., [17,18]).

To identify other quantities and/or methods that can provide useful insights for evaluating the lubrication behaviour of gearboxes, a bibliographic review was conducted to analyse the studies related to this article topic. Hence, engineering studies published in the last decade reporting experimental results on gear lubrication were reviewed. References that refer to the same project/test rig are considered as a single entry. A total of 63 entries had been evaluated. The review is summarised in Table 1.

Table 1
Literature review, references are sorted by publication year, from the oldest to the newest. The column “G.” refers to the entries that contain the gear geometry and the housing geometry, while “G. + H.” refers to the entries that contain both the gear and the housing geometry. The column “Eff.” refers to references containing efficiency data.

Ref.	Lub. type		Fluid	Available geom.		Exp. technique		
	Splash	Jet	Declared	G.	G. + H.	Eff.	Photo	Other
[19]	✓			✓	✓		✓	✓
[20,21]		✓		✓	✓	✓		
[22]	✓		✓	✓	✓		✓	✓
[23]		✓	✓	✓		✓	✓	
[24]		✓	✓				✓	
[25]	✓		✓	✓		✓		
[26]	✓		✓	✓	✓		✓	✓
[27]	✓		✓	✓				✓
[28]	✓		✓	✓		✓		
[29,30]		✓	✓	✓		✓		
[31]		✓	✓			✓		
[32]	✓					✓		
[33]	✓		✓	✓		✓	✓	
[34]		✓	✓	✓			✓	
[35,36]		✓						✓
[37,38]		✓	✓	✓	✓	✓		
[39]	✓		✓	✓		✓	✓	
[40,41]	✓					✓		
[42,43]	✓							✓
[44]	✓		✓	✓		✓	✓	
[45]	✓		✓	✓		✓	✓	
[46]	✓		✓	✓	✓	✓		✓
[47]		✓	✓	✓		✓		
[48]	✓	✓	✓	✓		✓		
[49]	✓		✓	✓		✓		
[50]	✓		✓	✓		✓	✓	
[51]	✓		✓	✓		✓	✓	
[52]		✓		✓				✓
[53]	✓		✓	✓		✓		✓
[54]		✓		✓		✓		
[55]	✓		✓			✓		✓
[56,57]	✓		✓	✓		✓		
[58]	✓		✓	✓	✓		✓	
[59]	✓		✓	✓		✓	✓	
[60]		✓	✓	✓		✓		✓
[61]	✓		✓	✓	✓	✓	✓	
[62]	✓		✓	✓		✓	✓	
[63]		✓		✓		✓		
[64]	✓		✓	✓		✓		
[65]	✓		✓	✓	✓	✓	✓	
[66]	✓		✓	✓				✓
[67,68]	✓		✓	✓		✓		✓
[69]		✓	✓	✓	✓			✓
[70]	✓		✓	✓			✓	
[71]	✓		✓			✓	✓	✓
[72]	✓		✓				✓	
[73]		✓	✓			✓	✓	
[74]		✓	✓	✓				✓
[75]		✓					✓	✓
[76]	✓		✓	✓		✓		
[77]	✓		✓	✓			✓	✓
[78]	✓		✓	✓		✓		
[79]	✓		✓	✓		✓		
[80]		✓	✓	✓				✓
[81]		✓	✓	✓				✓
[82]	✓		✓	✓		✓		
[83]	✓							✓
[84]	✓		✓	✓		✓		
[85]		✓					✓	✓
[86]	✓							✓
[87]		✓				✓		
[88]	✓		✓			✓		
[89]		✓	✓	✓				✓
Total	41	23	47	49	10	40	24	24

Here it must be noted that, among these more than 60 entries, 48 of them report the gears geometry. However, only 10 of them report the gearbox geometry as well. Hence, only for the latter group is it possible to completely replicate (numerically) the test as the complete geometry does not have to be devised. Among this latter group, only 5 articles (i.e., [20,21,37,38,69]) deal with jet lubrication. It is worth noting that [20,21,37,38] are based on the same test bench.

Almost a third of the works deals with experimental tests on jet-lubricated gears. That is, even on the experimental side, the jet lubrication case is less treated by the literature. More in detail, Handschuh and Hurrel [20,21] exhibit power loss data a single jet-lubricated gear while Arisawa et al. [23] evaluate the power losses of a bevel gear pair, with and without shrouding; they also report photographic analysis. Wang et al. [24] report high-speed recording of a spur gear, using water instead of a classical lubrication oil. Fernandes et al. [29,30] show an extensive campaign about the efficiency of spur gears. In a later work, Fernandes et al. [31] also present results on an entire wind turbine gearbox with jet-lubricated stages. Massini et al. [34] provid the evolution of an oil jet interacting with a spur gear at different rotational speeds. Wang et al. [35,36] focus on the cooling aspect of the jet, with a single measurement point of the measured tooth temperature. Delgado and Hurrel [37,38] show windage power loss data obtained using the test rig developed by Handschuh and Hurrel [20,21]. Power losses are also reported by Arisawa et al. [47] for an helical gear pair. Moss et al. [48] show efficiency data for spur gears with different nozzle configurations. Dai et al. [52] evaluat the trend of the tooth surface temperature using a thermal camera. Dindar et al. [54] report several tests about gearbox power losses with spur gears with different surface finishings. Andersson et al. [60] present efficiency and gear temperature data obtained on super-finished spur gears using a “classical” FZG gear test rig. Li and Wang [63] focus on power losses of a jet-lubricated spiral bevel gear. Torres et al. [69] report temperature data of a single jet-lubricated spur gear made in aluminium. Dai et al. [73] show high-speed recording of the oil flows generated by the impact of an oil jet on a face gear as well as power loss measurements. Jiang et al. [74] and Qiao et al. [80] report experiments similar to Dai et al. [52] but on different gear geometries and with different nozzle configurations. Suzuki et al. [75] and, later, Ohno et al. [85] focus on lubrication phenomena within high-speed gearbox for automotive applications, showing high-speed recording, (PIV) data and thermal analysis. Hu et al. [81] and Hu et al. [89] evaluate the temperature of a jet-lubricated herringbone gear pair. Lastly, Neuenfeldt et al. [87] show efficiency data of a jet-lubricated turbo gearbox.

The evaluation of Table 1 articles highlights two main methodologies employed for the analysis of gearbox lubrication: efficiency (or power/torque losses) measurements and photographic study of the meshing gears. Here, it must be noted that Cardozo et al. [84] improved the photographic analysis, obtaining a quantitative measure (i.e., the oil velocity field of a splash-lubricated gearbox) by using computer vision techniques.

These two techniques are adopted in most cases. However, photographic analysis allows only qualitative evaluation of the oil behaviour. On the other hand, the power losses of a gearbox are composed of several components (e.g. bearing and sealing losses). Additional tests and/or a dedicated test rig are necessary to discern the quantity that is specifically related to the fluid-dynamic interactions between the gears and the oil/air mixture inside the gearbox (e.g., [54,90]). As it is an indirect measure, efficiency is a quantity more prone to uncertainty. At the same, efficiency is a different phenomena, as it is a consequence of the oil flows.

There also exist alternative techniques, defined in the “Other” column of Table 1, which will be presented and discussed to derive the experimental technique adopted in this work. These alternative techniques can be classified into three main categories, as shown in Table 2

The first techniques in this series, certainly the most advanced and experimentally demanding, are (LDA) and PIV. LDA enables pointwise velocity measurements of air while PIV allows the acquisition of velocity fields in both 2D and 3D. LDA had been used by Simmons et al. [27] to measure the velocity of a fluid (i.e., air) passing through a calibrated hole located in the shrouding of a bevel stage of an aero-engine. PIV had been adopted as a means to evaluate fluid (i.e. air) flows around a single gear by Massini et al. [42,43] and a spur gear pair Suzuki et al. [75]. Chernoray’s research group used PIV on a single-stage spur gear transmission [19,22,26,53] with actual lubrication oil. However, those techniques require a transparent fluid (air or lubrication oil) to work properly, and the oil adopted here is coloured (specifically, light brown with purple hues). In any case, transparency is not a necessary condition for PIV as it can also be adopted with slightly coloured oils. Here, however, the main issue is the non-uniform density of the air-oil mixture that forms in jet lubrication. This alters the optical properties of the resulting two-phase fluid. Furthermore, it is necessary to suspend particles (often fluorescent) in the oil, which may modify the behaviour of the micro-droplets generated during lubrication. Hence, neither LDA nor PIV can be adopted in this specific case. Here, it must be noted that Cardozo et al. [84] is a first attempt to overcome such a limitation, exploiting the lubricant appearance to derive the velocity field.

Table 2
Summary of the “other” experimental technique.

Method	References
LDA and PIV	[19,22,26,27,42,43,53,75]
Thermal analysis	[35–37,52,55,60,66–69,74,80,85,86,89]
Oil collection	[46,51,71,77,83]

Another technique that provides useful information models is the analysis of the thermal behaviour of the gearbox [67,68,86], its lubricant [55,66,85] and/or of its subcomponents [37] and the gears [35,36,52,60,69,74,80,81,89]. Typical approaches include point measurements via thermocouples [35–37,55,60,67,68,81,86,89], as well as global measurements performed with infrared cameras [52,66,74,80,85,86]. It must be noted that this type of measurements are mainly applied to study the thermal effect that the oil has on the system/components rather than on the oil *per se*.

The last group of papers follows the idea of performing measurements directly on the oil. This set of works involves the design of expansion thanks and/or collection pockets from which point measurements of the oil can be performed. However, despite being very simple, it is adopted only by very few (and recent) studies. A first example is the works of Neurouth et al. [46] and of Quiban et al. [51], where a siphon is installed inside an oil bath agitated by a gear. In this case, the steady-state oil height within the siphon is used as the indicator. Kunik et al. [71] use an expansion vessel connected to the lower part of a vertically oriented two-stage epicyclic gearbox. Here, the measured quantity is the oil level inside the vessel. Hildebrand et al. [77] perform point measurements by observing the amount of oil collected and subsequently removed through an extraction channel. A similar concept is adopted by Reichl and Lenz [83], who perform measurements inside a single-stage helical-gear reducer. Specifically, they use a “riser tube” (*sic*), essentially a Pitot tube, placed near the gear to measure the oil level, and, in another configuration, they employ “tangential oil catchers” (*sic*) located tangentially to the gear. In this case, the measurement corresponds to the amount of oil collected over time.

It should be noted that, under splash lubrication, oil collection and extraction disturb the equilibrium of the oil bath. By contrast, this approach appears well suited to the investigation of jet lubrication, where oil extraction is required for recirculation. For this reason, the present study considers extraction points located downstream of the oil jets as a practical means of obtaining a quantitative metric, namely the amount of oil collected at each port over a given time interval. This method offers several advantages: it provides quantitative data, unlike photographic analysis; it is based on a direct measurement, unlike

Fig. 1. Test rig in its original configuration.

efficiency-based approaches; it is applicable to any lubricating oil; and it does not require a complex experimental arrangement, unlike PIV or LDA.

This methodology yields information only on the region associated with each pocket and does not describe the overall flow behaviour. In contrast, photographic analysis makes it possible to observe the global flow pattern, although only in a qualitative sense. Therefore, the quantitative, but localized, information obtained with the present method should be complemented by the qualitative yet global evidence provided by photographic observations.

For these reasons, the proposed test rig will include shrouds surrounding two spur gears. Several pockets will be defined within the shrouds, and the oil discharged from each pocket will be collected and measured. Optical access to the entire housing will be provided by a transparent panel.

3. Development of the test rig

The developed test rig is based on the "CENIT2" test rig, which is a four-square gear testing machine with a 91.5 mm centre distance, operating in a closed-loop configuration (back-to-back). A picture of the test rig is shown in Fig. 1. Unlike the classical FZG test rig, "CENIT2" applies the load (i.e., torque) by means of a rotating hydraulic actuator, and the adopted gear ratio is 17/18. As is typical of geared test benches, it includes a dedicated system for controlling the lubricant temperature before it enters the gearboxes. A description of the basic principle of back-to-back test rigs can be found in [91]. In the present work, the test gearbox was redesigned, and both the housing and the final section of the lubrication system were modified to satisfy the requirements of the experimental campaign. Only one half of the original test-gearbox housing, bolted to the steel base, was retained, whereas all rotating components, including shafts and bearings, were newly designed.

The test rig already available imposes dimensional constraints on the gears (module and number of teeth) as well as other minor geometrical constraints (e.g., housing maximum dimensions and nozzle position with respect to the gear axis). Efforts were therefore made to obtain within the design geometry and lubrication configurations as close as possible to the real MGB application. Hence the choice of the oil used (i.e., AeroShell Turbine Oil 555), the 1 mm diameter nozzles pointing towards the meshing region, the target nozzle pressure of 4 Bar and the peculiar housing structure with its shrouding.

To avoid gear rattle, tests are performed with a very low torque under the assumption that the active load does not influence oil-related phenomena (e.g. [92,93]). Hence, the shafts are kept overhanging, supported by two radial ball bearings housed in cartridges placed within the housing. This allow for the complete optical access to the meshing region and its surrounding. Shielded bearings are used to avoid to lubricate them, hence avoiding interference with the flows related to the gear meshing process. The gears are connected to the shaft via a parallel key and secured in the axial direction by a shaft cover.

The transparent panel provides optical access to the gearing and features two openings aligned with the jet nozzles, allowing for their adjustment. The two nozzles are mounted into the housing, above and below the gear meshing region, and oriented toward the meshing region.

The assembly of the new casing consists of several laser-cut plates stacked together to define the internal geometry, plus a rear plate with tapered edges adjacent to the housing frame. A structural front plate closes the stack and connects the assembly to the housing frame. Each internal plate contains the collection pockets with corresponding drainage channels. Raised edges around each pocket serve as physical separators, ensuring that the oil collected by each pocket originates from its designated area. Liquid sealing is adopted to seal the whole structure.

The drainage channels at the base of each pocket direct the oil toward the ports machined into the front plate. The latter does not present channels; instead, it closes the internal geometry and provides threaded connections for outlet fittings and for mounting the transparent panel. The fittings drain the oil into the graduated cylinders. The collected oil, measured over fixed intervals, forms the quantitative dataset discussed here.

The shrouding shape had been defined based on internal knowledge and on the features of the test rig. A sketch of the housing is shown in Fig. 2, while a section view is shown in Fig. 3. The geometry of the test rig is designed to be symmetric with respect to a plane passing through the gear face midplane. In fact, the symmetry of the structure itself is *conditio sine qua non* for applying symmetry in any numerical model.

The step file of the test rig is included in the supplementary material of the article while a sketch with the basic dimension is shown in Fig. 4.

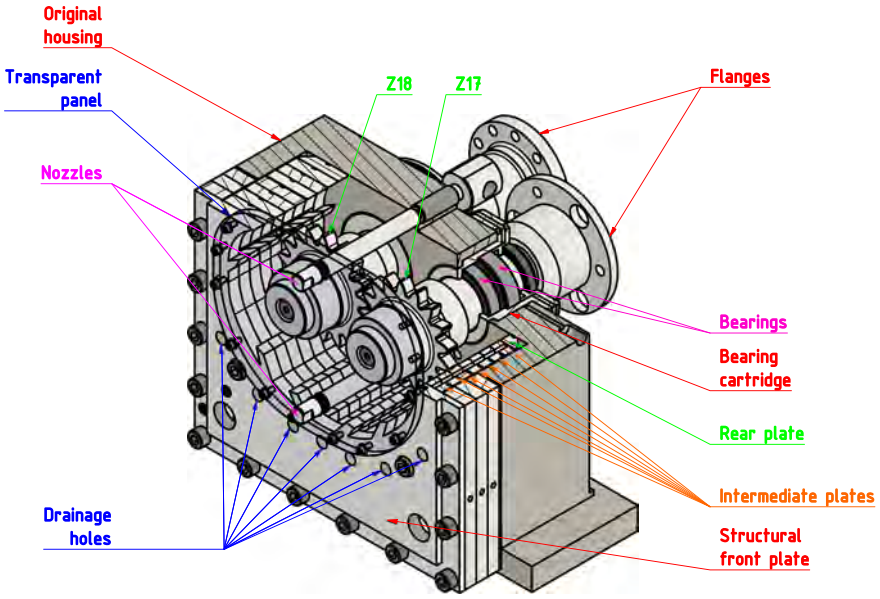

Fig. 2. Housing detail.

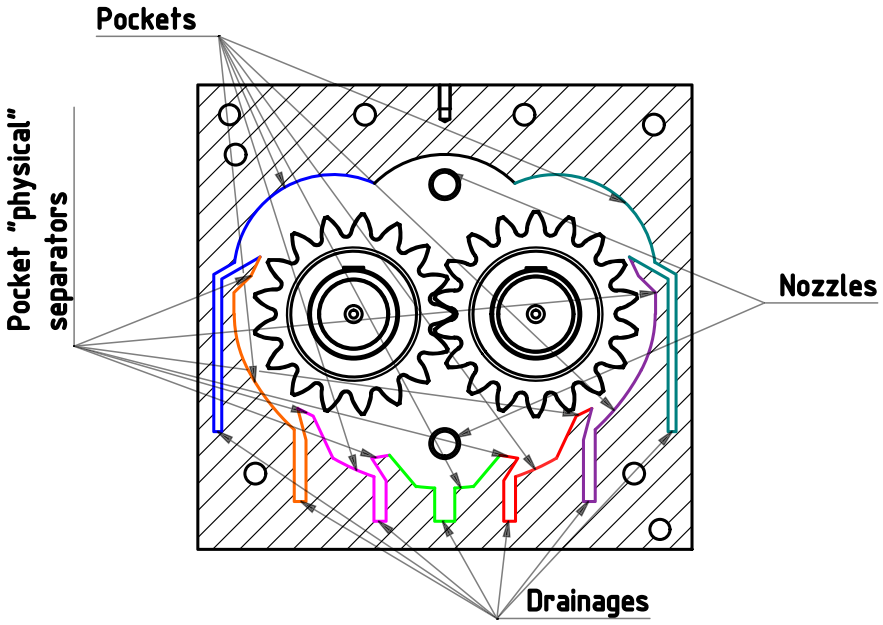

Fig. 3. Housing section. A different coloring highlights the different collective pockets and their drainage channel.

Fig. 5 presents two views of the test bench during the high-speed video recordings. In particular, Fig. 5-(a) shows the complete set-up, including the camera and the associated lighting system. The vertical blue panel contains the oil flow control system. Fig. 5-(b) shows the front view of the rig together with the camera field of view. In this image, the oil drainage pipes are also clearly visible. During tests performed with video acquisition, these pipes discharge the oil into a bucket (and not into the dedicated graduated cylinder).

4. Test campaign

The following test procedure was defined for the oil collection measurements:

1. Activation of oil jets and shaft rotation.
2. Timed operation for 5 min.
3. Shutdown and collection of residual oil.

After assembling the test bench, a functional verification was performed. The inspection focused on system integrity, confirming the absence of oil leakage between components and proper drainage across all channels. Additional tests assessed the system transient time, which includes the time required to reach the target rotational speed and the time needed for the oil to get to the graduated cylinders after nozzle activation. In worst-case conditions, this delay was estimated to be ≈ 20 s. These tests showed that the variability between repeated measurements of the oil volume collected in each graduated cylinder was equal to the cylinder resolution, namely 50 ml [94]; this correspond to ≈1% of the almost 4000 ml of oil passing throughout each single nozzle during the 5 min of operation.

Tests were conducted on the geometry of interest, referred to as “A”, and on a second geometry already available and compatible with the test bench, referred to as “B”. From a geometric standpoint, the gears are globally similar (same number of teeth and module) but differ in profile shift, implying different tip diameters (i.e., [95]), and in face

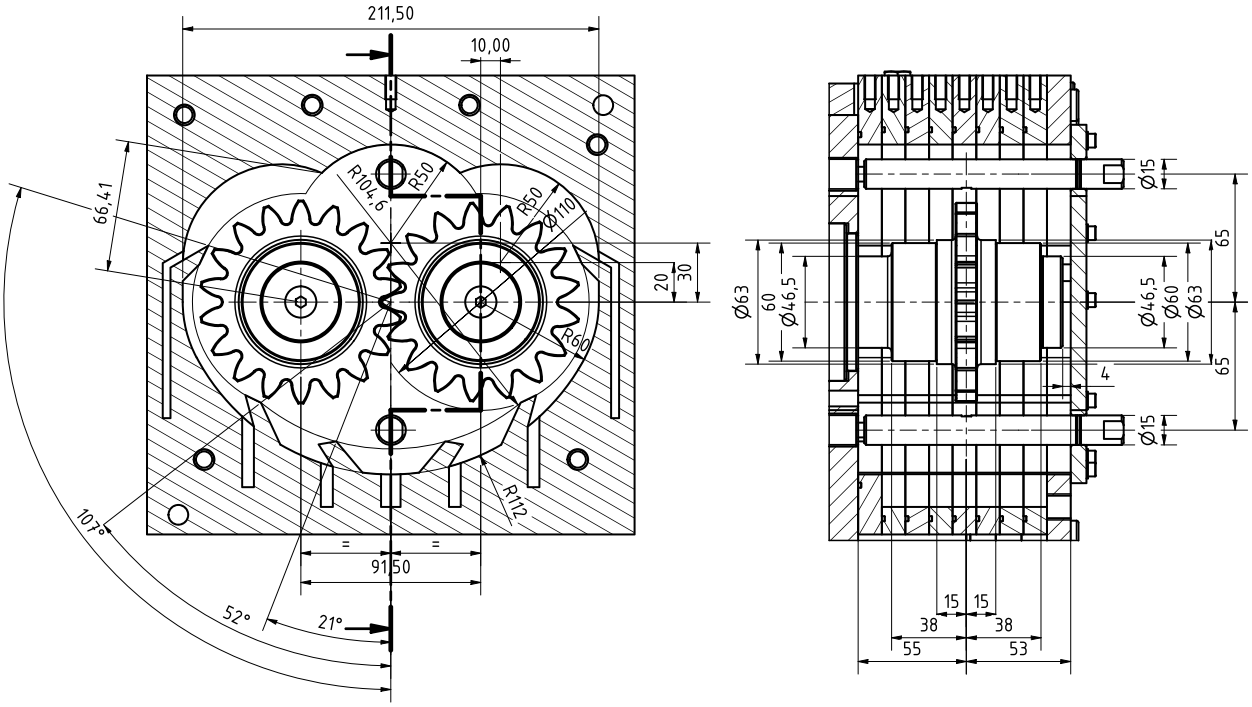

Fig. 4. Housing section with basic dimensions.

Table 3
Gear geometries.

		A		B		
		Z17	Z18	Z17	Z18	
Number of theet	Z	17	18	17	18	–
Normal module	m_n	5		5		mm
Center distance	a	91.5		91.5		mm
Pressure angle	α	20		20		°
Face width	b	11	12	12.5	12.5	mm
Profile shift	x	0.466	0.454	0.475	0.445	–
Reference diameter	d	85	90	85	90	mm
Root diameter	d_f	78.37	80.34	75.75	80.45	mm
Root radius	ρ_{Fp}	2.4	2.6	1.5	1.5	mm
Tip diameter	d_a	101.1	103.07	99.75	104.45	mm

Table 4
Average nozzle flow rate.

T	p	Flow rate
°C	Bar	L/min
60	3	0.75
60	4	0.85
60	5	0.95
90	4	0.90

widths. The geometries of the two gear sets are summarised in Table 3. The gear body is the same for both geometries and is included in the step file of the test rig.

The main experimental campaign focused on analysing the behaviour of geometries “A” and “B” within the test bench speed range, in 500 rpm increments and in both rotation directions (i.e., (CW) and (CCW)). Tests were performed at six speed levels: 500, 1000, 1500, 2000, 2500, and 3000 rpm, under three nozzle configurations: only upper nozzle active, only lower nozzle active, and both active. In this setup, nozzle pressure was set to 4 bar to replicate application conditions, with a test temperature of 60 °C. A total of 72 test conditions had been evaluated. A subsequent series of tests was carried out on geometry “A” at the two extremes of the speed range, again in both rotation directions and with the three nozzle configurations. These tests investigated the effect of varying nozzle pressure (3 and 5 bar) while keeping the test temperature of 60 °C, and the effect of increased oil temperature (90 °C), while maintaining nozzle pressure at 4 bar, leading to 24 different test conditions. A total of 96 test conditions had been analysed, with each test repeated 2 times. The oil adopted for these analyses is the “AeroShell Turbine Oil555”, which is the mineral oil adopted in the actual application (i.e. the MGB).

The quantitative analysis of the oil flow is complemented by a qualitative investigation based on high-speed imaging, as shown in Fig. 5. A Phantom VEO-E 310L high-speed camer was used to record the lubrication phenomena while two 450 W LED lamps provide the proper illumination. Images were acquired at 7500 fps. This corresponds to ten times the meshing frequency at 3000 rpm (750 Hz). High-speed photographs and video recordings were collected for gearing “A” at six rotational speed levels, for different nozzle configurations, and for both directions of rotation.

5. Experimental results

The nomenclature of the tests is described in Fig. 6. Rotation directions (i.e., CW and CCW) are defined on the pinion (i.e., Z17). The two nozzles (i.e., upper and lower) point towards the meshing region. Hence, when the rotation is CW, the lower nozzle is “in-mesh” while the upper one is “out-of-mesh”; when the rotation is CCW, it is *vice versa*: the upper nozzle is “in-mesh” while the lower is “out-of-mesh”. All results discussed here are presented as averaged and as percentages of the total oil flow.

The results of the main test campaign are shown as colour maps in Fig. 7 for Geometry “A” and in Fig. 8 for Geometry “B”. Each figure also reports the corresponding percentage values. The results of the tests performed with different nozzle pressure settings or lubricant temperatures are presented in Appendix A. The average nozzle flow rates at the different test conditions are reported in Table 4.

Several videos are also included, and are reported in Figs. 9–15. All videos are slowed down by a factor of 240 with respect to the actual phenomena. A frame for every single test condition of the main test

(a) *Side view*

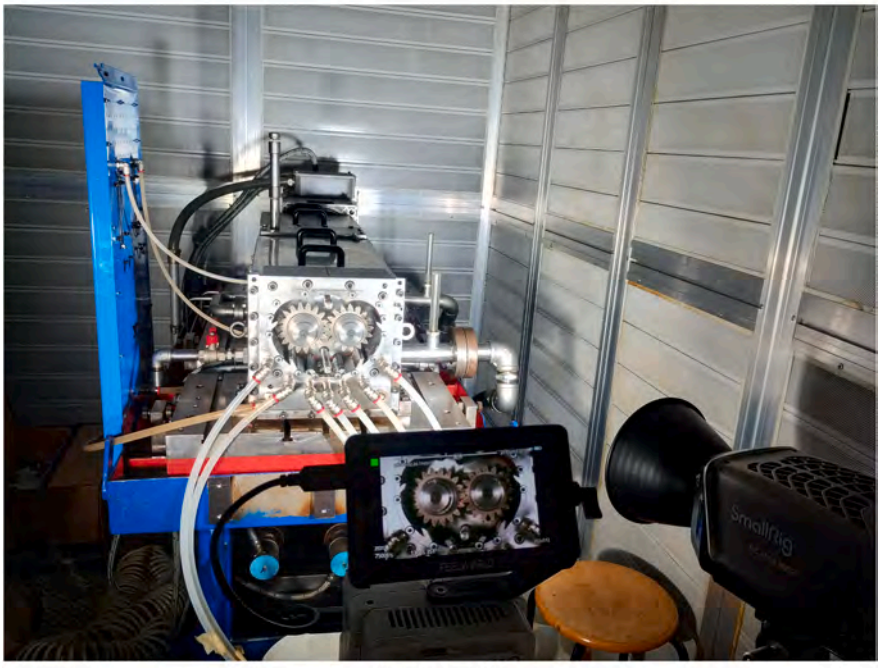

(b) *Front view*

Fig. 5. Experimental setup during high-speed camera recording.

campaign on gearing "A" are reported in Appendix B. Post-processing techniques had been applied to improve oil visibility. In the videos, the presence of oil flows centrifuged by the teeth can be discerned (especially at low speed), along with the formation of oil droplets originating from the upper cusps (on the side of the upper nozzle).

Fig. 6, reported without annotations in Appendix B and presented as a video in Fig. 15, illustrates the value of the proposed test rig. At the relatively high rotational speed shown in the figure (3000 rpm), the oil jet breaks up into droplets that are too small to be clearly resolved, which makes the actual flow paths difficult to identify. A similar limitation arises when oil is splashed onto the inspection panel, thereby reducing optical access to the housing interior. By contrast, the adopted experimental arrangement makes it possible to assess the oil flow by measuring the quantity collected in each pocket, providing useful information even when the flow cannot be fully visualised.

6. Discussion

By examining the oil distribution in the cases with a single active nozzle (i.e., Figs. 7-(a) to (d) and i.e., 8-(a) to (d)), it can be seen that, as expected, the main parameters governing the distribution are functional parameters: the direction of rotation (i.e., CW and CCW) and the active nozzle (i.e., upper and lower). Nevertheless, some global trends can be identified. CW rotation (i.e., Figs. 7-(a),-(c), 8-(a) and 8-(c)) promotes a

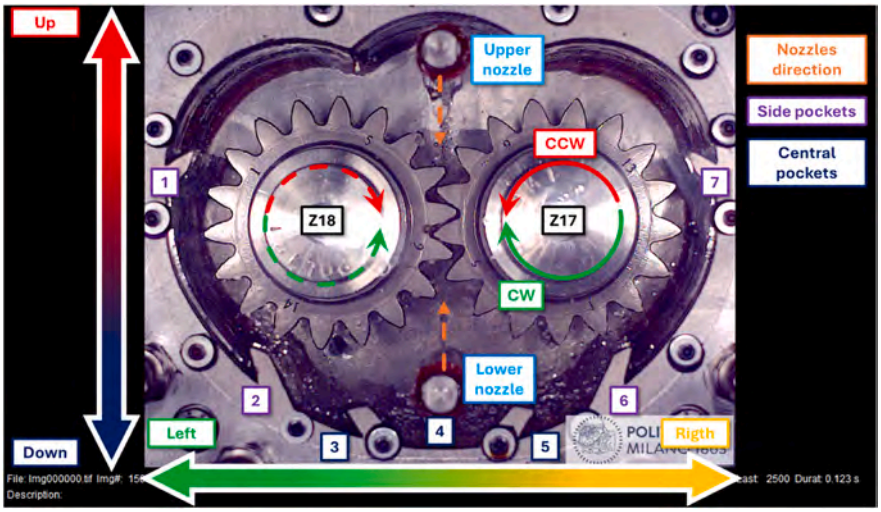

Fig. 6. Test nomenclature. The picture refers to a case at 3000 rpm, CCW, with both nozzles open.

more even division of the flow among the various pockets. On the other hand, when the rotation is in CCW (i.e., Figs. 7-(b), -(d), 8-(b) and -(d)), the distribution tends to concentrate in the central pockets (i.e., 3, 4, and 5).

To understand the reason for such behaviour, it is necessary to observe how the rotation directions are defined in Fig. 6. In the case under consideration, CW pushes the oil toward the upper part of the housing and thus toward the outer pockets (i.e., 1, 2, 6, and 7) as well. Conversely, CCW promotes a downward displacement of the oil, thereby limiting the amount of oil that can reach the outer pockets.

To this information, we can add the effect of the active nozzle position relative to the meshing direction. When the active nozzle is out-of-mesh (i.e., Fig. 7-(a), -(d), Fig. 8-(a), and -(d)), the oil jet impacts the tooth flanks moving in the opposite direction. This interaction disrupts the jet integrity. In the case of the upper active nozzle with CW rotation (i.e., Figs. 7-(a) and 8-(a)), the jet disruption occurs in the upper region of the housing and, combined with the rotation direction, the broken jet is further shifted laterally. Similarly, when the lower nozzle is active with CCW rotation (i.e., Figs. 7-(d) and 8-(d)), the jet disruption occurs in the lower part of the housing. Given the rotation direction, the disrupted jet ultimately falls predominantly into the more central pockets.

On the other hand, when the active nozzle is the in-mesh one (i.e., Figs. 7-(b), -(c), 8-(b), and -(c)), the jet is less disturbed by the meshing process, as the teeth move in a direction consistent with the jet itself. In the case of the upper active nozzle and CCW rotation (i.e. Figs. 7-(b) and 8-(b)), this causes the flow to reach mainly the central pocket (approximately 40%) and, aided by the rotation, the adjacent pockets. Similarly, when the lower nozzle is active (and the rotation is CW, i.e. Figs. 7-(c) and 8-(c)), the central pocket again collects the largest amount of oil. In this case, however, the rotation causes the gear to push the oil toward the more lateral pockets, to the detriment of those adjacent to the central pocket.

Evidence of this behaviour can also be found by examining the frames extracted from the high-speed recordings, particularly those acquired at low rotational speeds, namely 500 and 1000 rpm. In the case of out-of-mesh nozzles, the images show a highly disturbed region, that is, an area with a significant presence of oil splashed on the transparent screen, whose origin is shifted relative to the meshing zone. This occurs because the impact between the oil jet and the rotating teeth, on average, does not take place in the region upstream of the jet direction and, in the out-of-mesh configurations, the tooth flanks move in a direction opposite to the jet. This results in a more intense interaction between the oil jet and the tooth flanks. In the CW rotation case (i.e., Figs. B.1-(a) and B.3-(a)), this phenomenon is more pronounced than in its counterpart of lower nozzle active with gears in CCW direction (i.e., Figs. B.2-(b) and B.4-(b)). Indeed, as discussed above, the gears rotation in CW drives the oil toward the upper part of the housing, i.e., in a direction opposite to gravity. Conversely, with the in-mesh nozzles, the magnitude of the phenomenon is considerably smaller; furthermore, the disturbance originates much closer to the meshing region

Looking to the video recordings, it is possible to notice also this disruption of the oil jet, as shown in the videos referenced in Figs. 9 and 11. This phenomenon occurs in the region close to the meshing zone, specifically in the area above the mesh for Fig. 9 and in the area below the mesh for Fig. 11. By examining the flow behaviour in these upper and lower regions, the progressive meshing of the teeth leads to the formation of open volumes relative to the oil jet. As soon as these volumes open, the jet passes through them and impacts against the flank, dispersing the oil in multiple directions. On the other hand, when the active nozzle is in-mesh configuration, this phenomena does not occurs, as reported in the video Fig. 10.

The way in which the jets interact with the gears rotation and the resulting flow distribution do not depend solely on the active nozzle and the rotation direction, but also on the rotational speed, although to a lesser extent. It is therefore possible to address the first research question by examining the colour map (and the corresponding magnitude) associated with the data reported in Figs. 7 and 8. The results clearly show that a gradual variation in the amount of oil collected by the individual pockets does indeed occur; however, this variation does not modify the relative positioning between the central and lateral pockets.

A qualitative indication of this gradual effect of the rotational speed can also be observed in the frames reported in Appendix B. The oil-spray pattern on the viewing screen changes progressively as the rotational speed increases. For instance, in the case of the lower nozzle under CW rotation, spray formation is clearly visible at low speeds. Its intensity decreases as the rotational speed increases and ultimately disappears at 3000 rpm. It is possible to observe this effect also in the videos reported in this article, by comparing, for example, the one of Fig. 10 with the one of Fig. 13, the one of Fig. 11 with the one of Fig. 14, and the one of Fig. 12 with the one of Fig. 15.

Moving to the cases with two active jets (i.e., Figs. 7-(e), -(f), 8-(e) and -(e)) it is possible to address the second research question: the effect of having both an in-mesh and an out-of-mesh nozzle operating simultaneously. In these cases, the nozzle selection is removed as a discriminating factor; the only remaining variable is the direction of rotation. In this configuration, the quantitative outcome is consistent with the

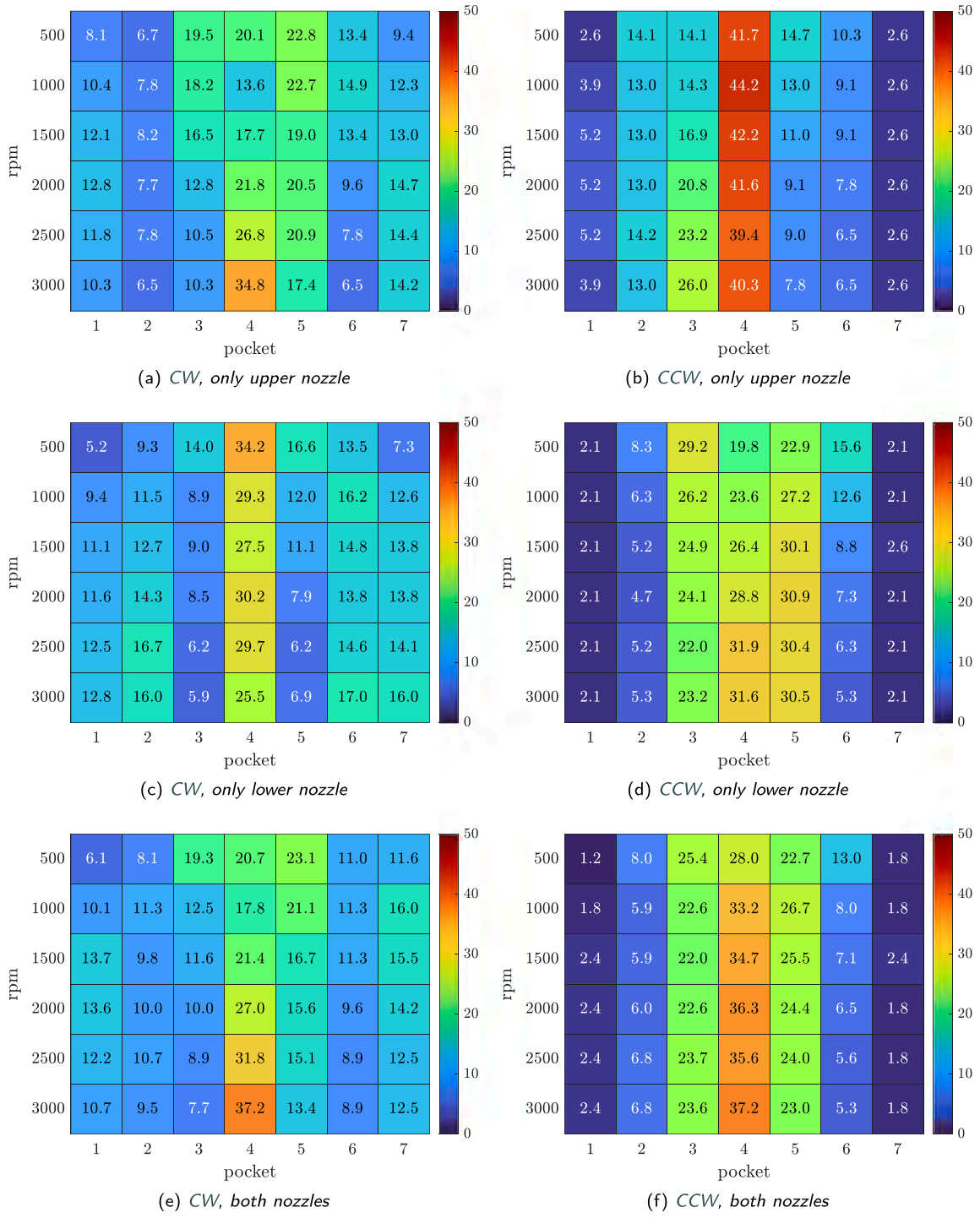

Fig. 7. Experimental results for gearing "A", T = 60 °C and p = 4bar.

single-jet cases: CW rotation moves the oil also to the lateral pockets, whereas CCW rotation favours the central pockets.

Once the above trends are established, the next step is to determine whether any interaction exists between the two jets and whether such interaction is strong enough to introduce nonlinearity into the system. To assess this, the principle of superposition was applied: the absolute results from the two single-jet configurations were summed and compared with the corresponding experimental distribution obtained with both jets active. Fig. 16 illustrates some examples of these outcomes, together with the error between the predicted value (i.e., the sum of the two single-jet flows) and the measured one. The distributions are highly similar, without significant change in the relative positioning of the pockets. To quantify this phenomenon, the (MAE) was computed across all test conditions presented here. The resulting MAE is 164 ml, corresponding to 4% of the ≈ 4000 ml of inlet oil from a single nozzle.

A qualitative indication of this phenomenon also emerges from the high-speed recordings, specifically the oil splashing on the observation screen. In the double-jet configuration, both the appearance and location of the oil splash are directly related to those observed in the corresponding single-jet cases. For example, at 500 rpm in CW rotation, the upper nozzle produces spray in the upper region, see Fig. B.1-(a) and the video of Fig. 9,. On the other hand, when the lower nozzle is active, the

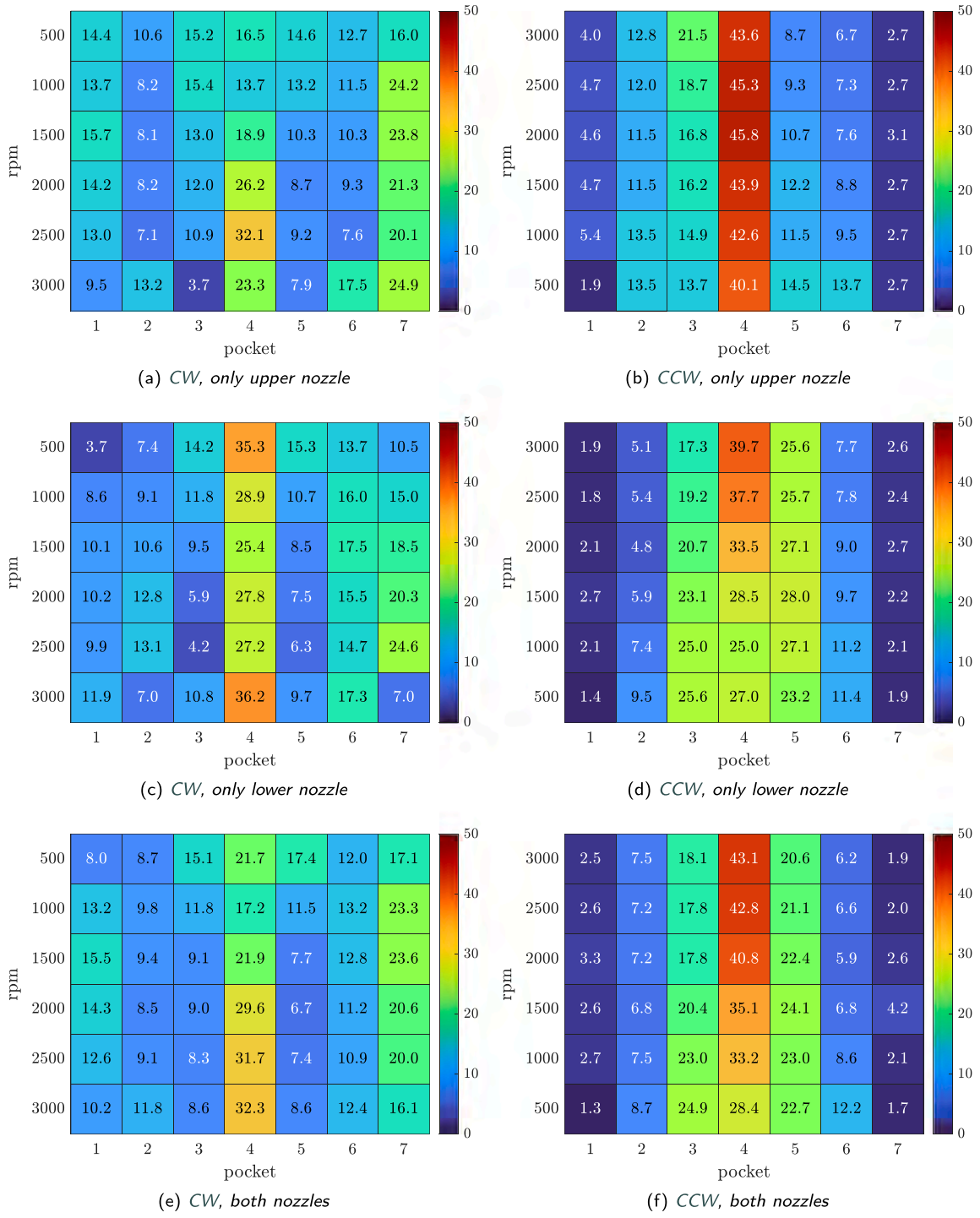

(a) *CW, only upper nozzle* (b) *CCW, only upper nozzle*

(c) *CW, only lower nozzle* (d) *CCW, only lower nozzle*

(e) *CW, both nozzles* (f) *CCW, both nozzles*

Fig. 8. Experimental results for gearing "B", T = 60 °C and p = 4bar.

splashing occurs in the central area, see Fig. B.1-(b). With both jets active, both regions show spray, see Fig. B.1-(c). At 500 rpm in CCW, the condition with the upper nozzle produces splashing in the lower and central part, see the video of Fig. 10, while the lower nozzle only in the lower part, see the video of Fig. 11, albeit to a lesser extent. When the two nozzles are active, the splashing occurs only at the lower and central part, see the video of Fig. 12. Similarly, at 3000 rpm in CCW rotation, no spray is present in the single jet cases, see the videos of Figs. 13 and 14, nor with two jets, see the videos of Fig. 15.

The limited interaction between the jets is due to the fact that the jets are physically separated by the continuous meshing of the gear teeth, which prevents the jets from interacting directly with each other. Indeed, as can be seen in the videos referenced in Figs. 9–11, 13, and 14, the jets do not cross the meshing zone for obvious physical reasons. As a consequence, any interaction occurs only after the jets have been disrupted by impact against the flanks.

By comparing the data presented in Figs. 7 and 8, it is possible to address the third research question, namely the influence of gear geometry. In this case, the two gear geometries are essentially equivalent, see Table 3, as they share the same module, number of teeth, and nearly identical face width. The only difference arises from different profile shifts, hence the different tip diameters [95]. A simple macroscopic

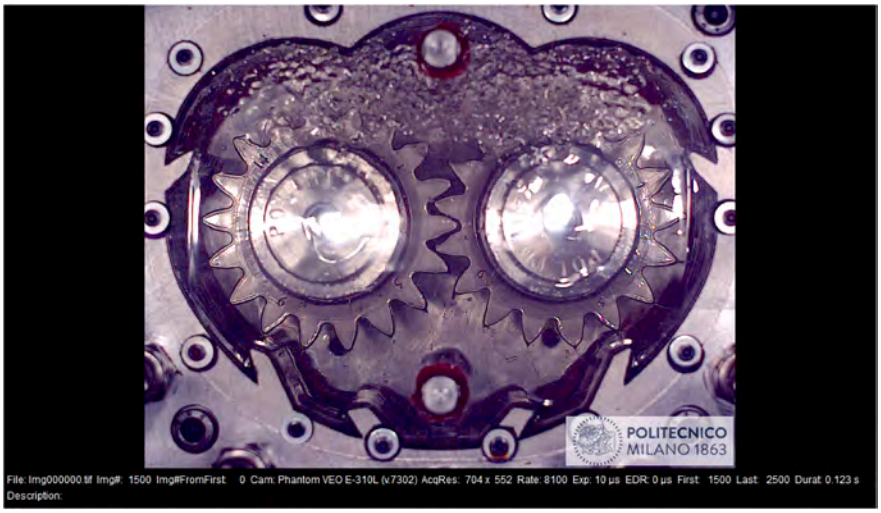

Fig. 9. Video recording of the case at 500 rpm, CW with only the upper nozzle active.

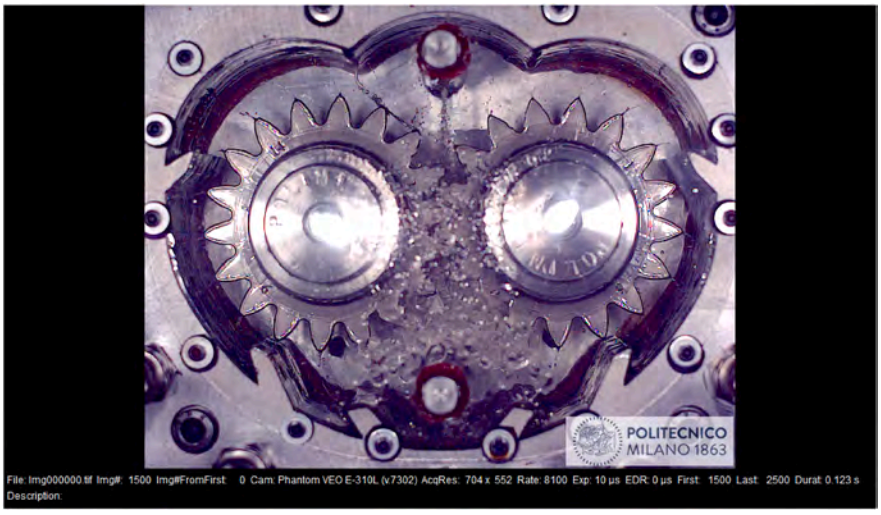

Fig. 10. Video recording of the case at 500 rpm, CCW with only the upper nozzle active.

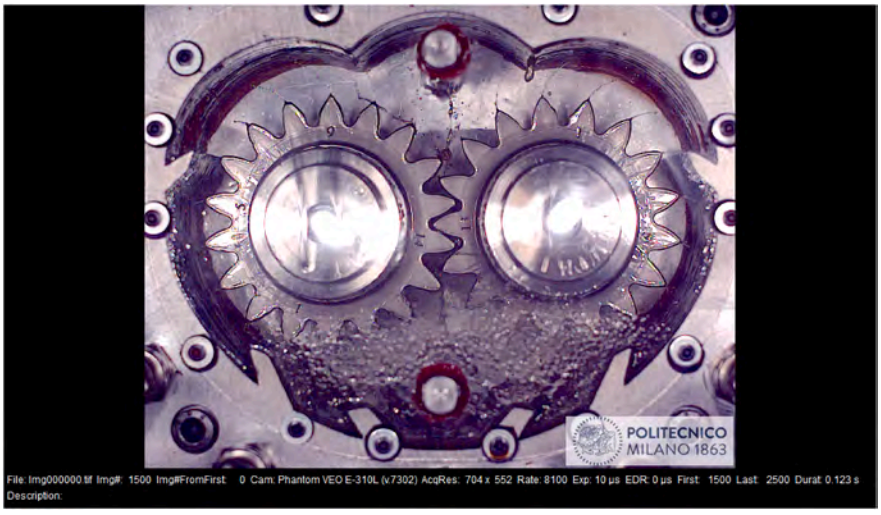

Fig. 11. Video recording of the case at 500 rpm, CCW with only the lower nozzle active.

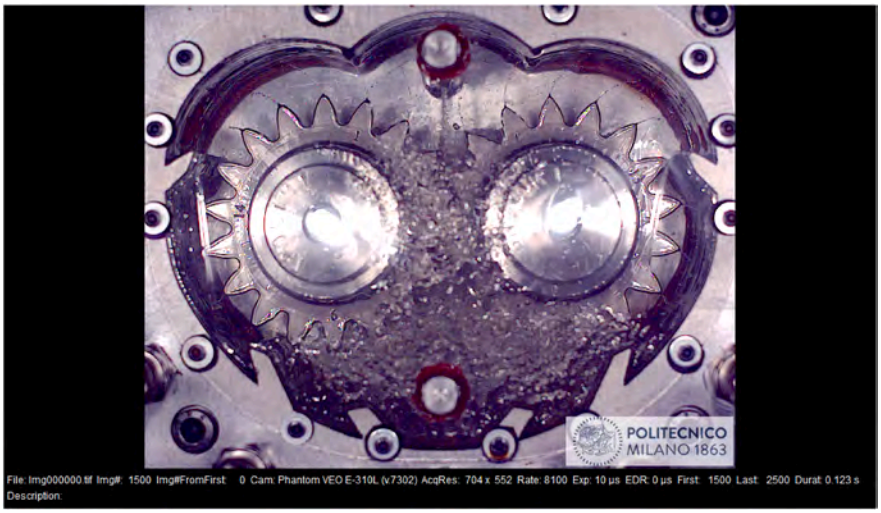

Fig. 12. Video recording of the case at 500 rpm, CCW with both nozzles active.

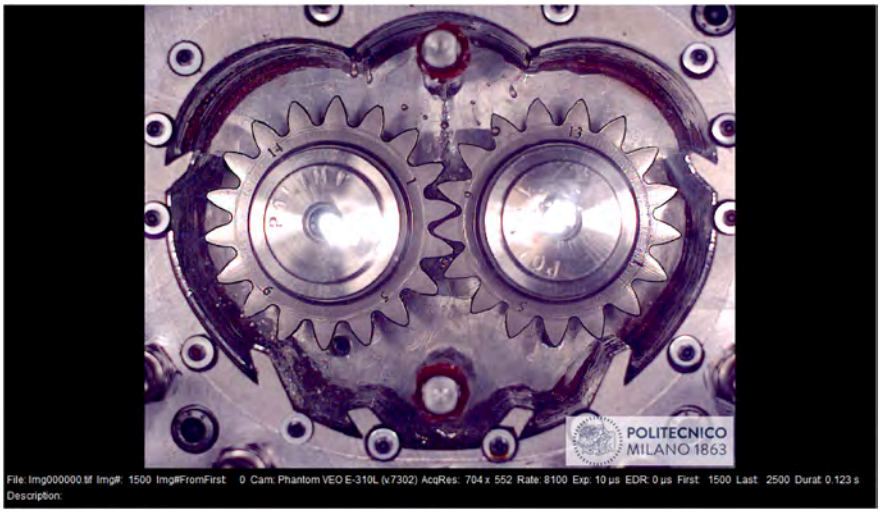

Fig. 13. Video recording of the case at 3000 rpm, CCW with only the upper nozzle active.

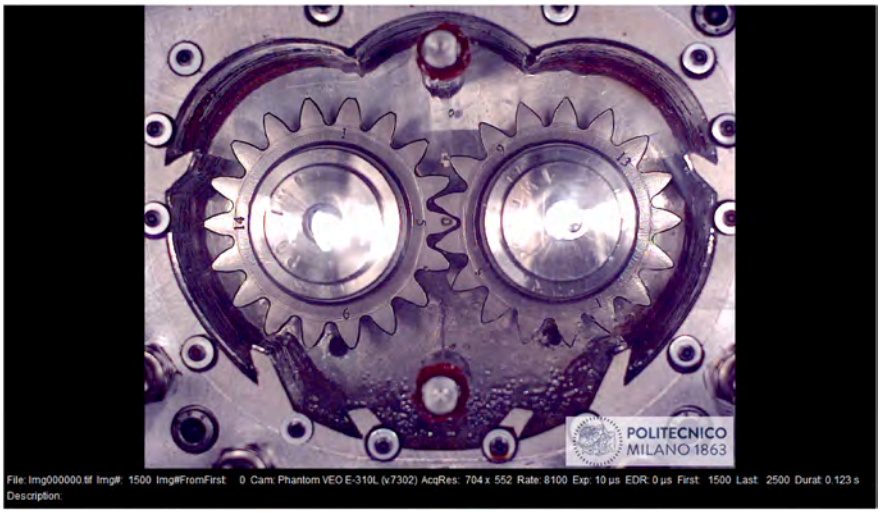

Fig. 14. Video recording of the case at 3000 rpm, CCW with only the lower nozzle active.

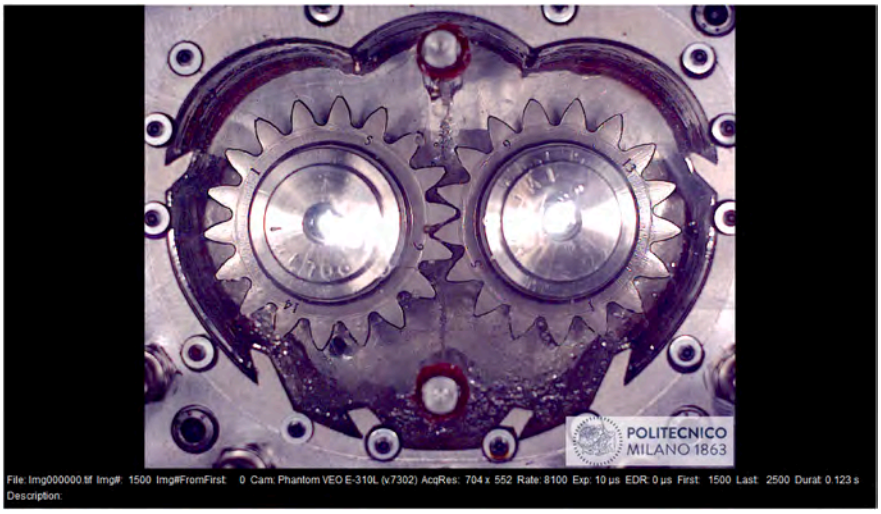

Fig. 15. Video recording of the case at 3000 rpm, CCW with both nozzles active.

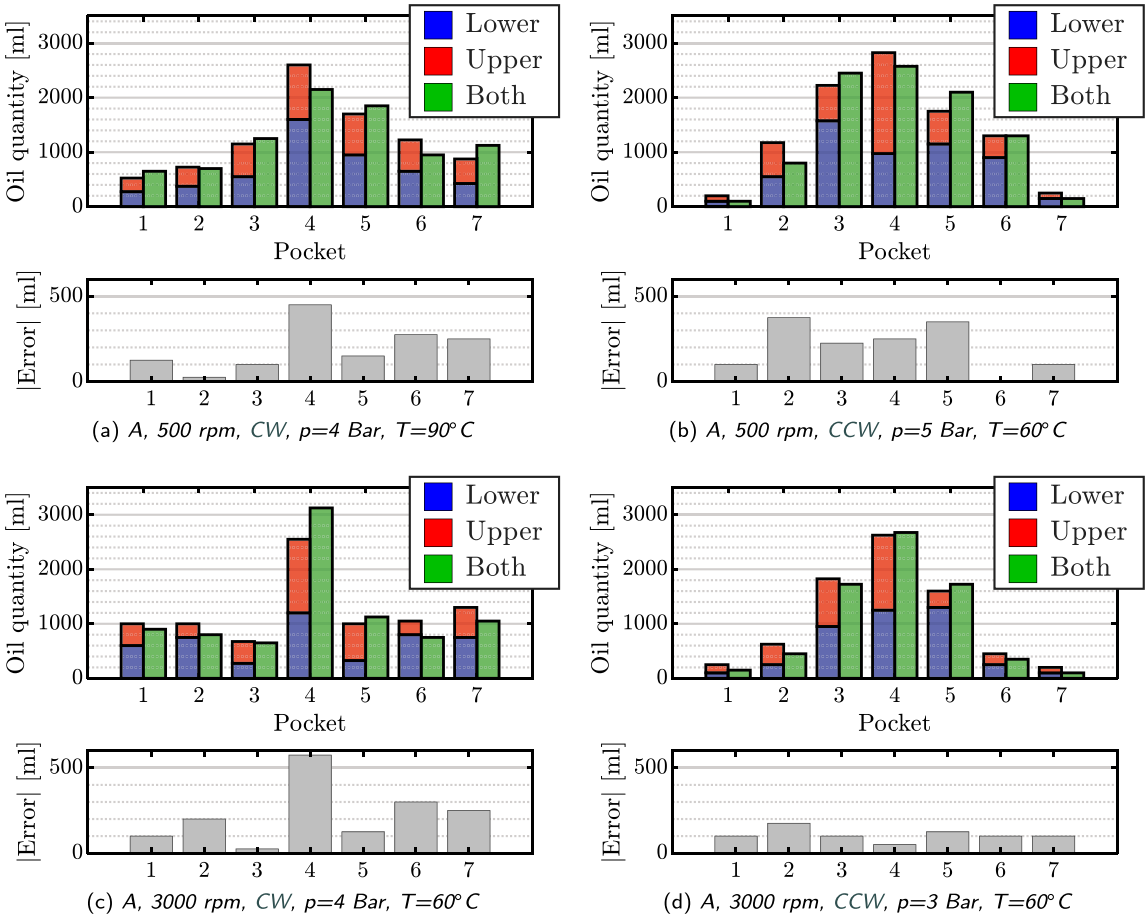

Fig. 16. Superimposition principle. Data are for four different test conditions. Each single figure presents the direct comparison above, while the absolute error is reported below.

comparison of Figs. 7 and 8 data suggests that simple geometrical differences do not alter the overall behaviour: CW rotation still leads to oil flows more distributed among the pockets, whereas CCW rotation favours the central pockets at the expense of the lateral ones. A more detailed analysis, however, reveals that geometry "A" exhibits more "symmetrical" flows, while geometry "B" favours the side pockets on the right over the left ones, especially in the CW case (where gear rotation pushes the oil upward) and the upper nozzle active.

The reason for this behaviour is related to the different tip diameters of the two geometries. In geometry "A", the tip diameters are much more similar to each other than in geometry B, as can be seen from the data reported in Table 3. By contrast, the pocket geometry is symmetric with

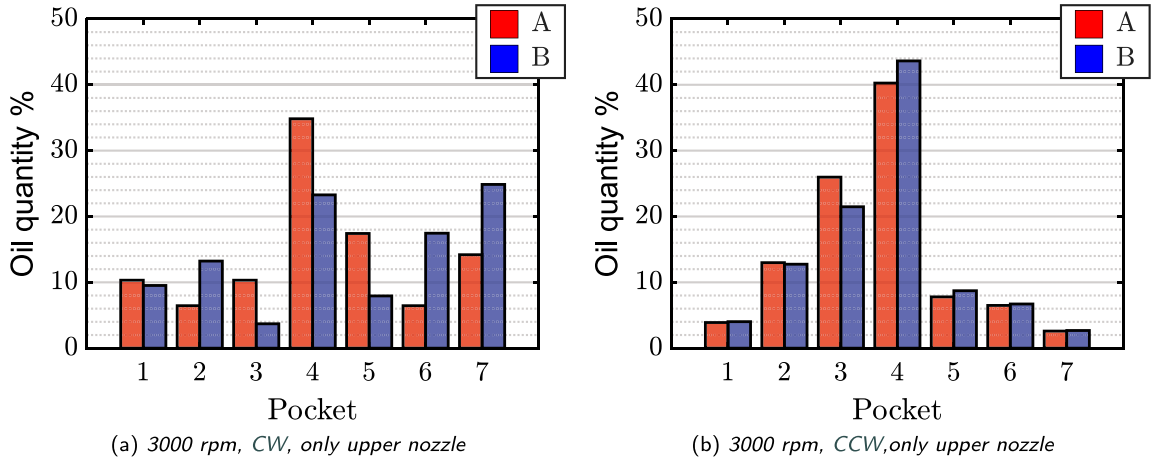

(a) *3000 rpm, CW, only upper nozzle* (b) *3000 rpm, CCW,only upper nozzle*

Fig. 17. Comparison of results obtained for "A" and "B" geometries. Data are for p = 4 Bar and T = 60 °C.

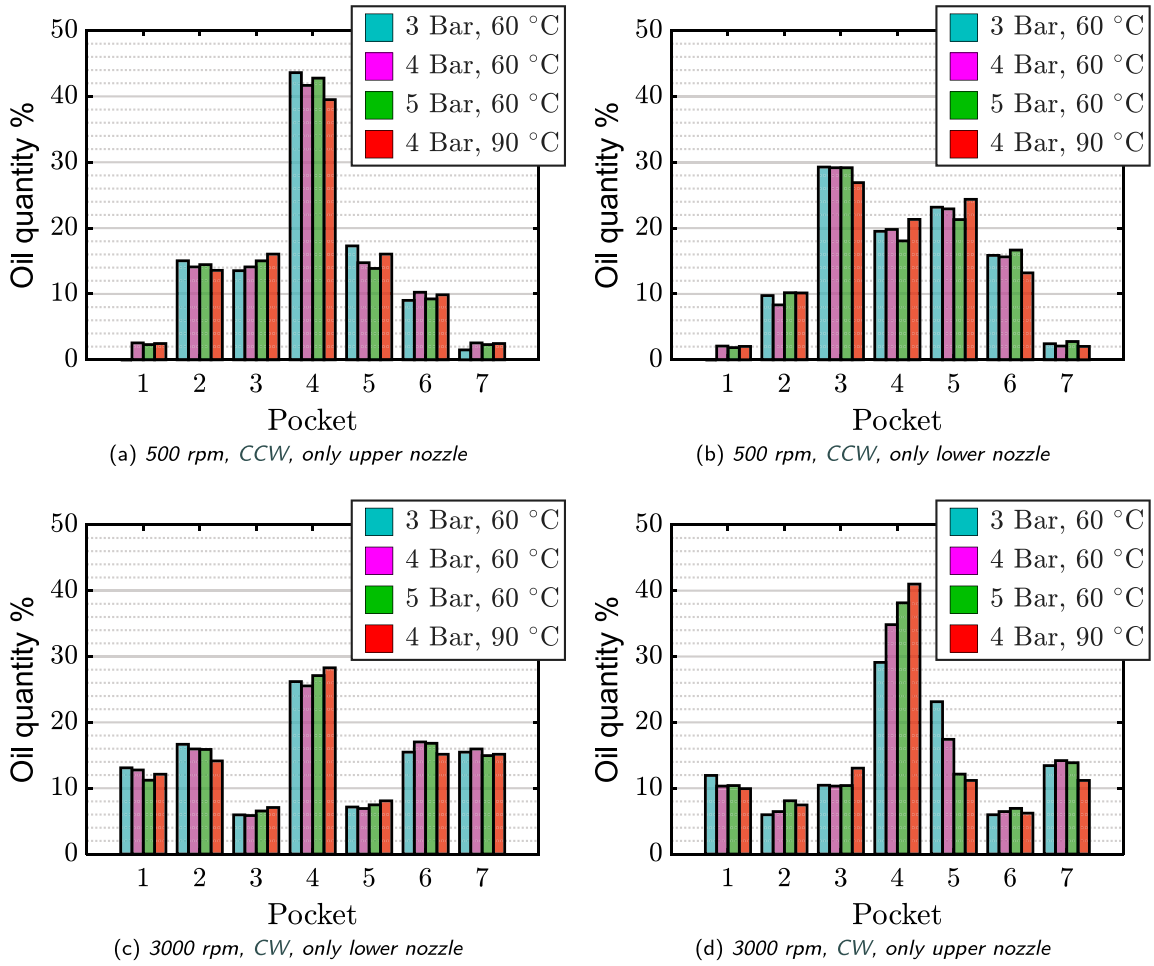

(a) *500 rpm, CCW, only upper nozzle* (b) *500 rpm, CCW, only lower nozzle*

(c) *3000 rpm, CW, only lower nozzle* (d) *3000 rpm, CW, only upper nozzle*

Fig. 18. Test results obtained by varying the test conditions.

respect to the vertical axis, see Fig. 4. This also implies that the spaces available between the two upper cusps and the tip diameters are much more similar (and symmetric) in case "A" than in case "B", leading to more "symmetrical" oil flows within the housing. As a result, the resulting oil flow patterns may differ when such openings are involved (i.e., in CW with upper nozzle active), as shown in Fig. 17. In Fig. 17-(a) (CW with only upper nozzle active), pocket 7 shows, for gearing (B), a flow whose magnitude becomes comparable to that of the central pocket, whereas this effect is not so pronounced for gearing "A". On the other hand, Fig. 17-(b) (CCW with only upper nozzle active) show more similar results between the two gearing. Comparing the values reported in Figs. 7-(a) and 8-(a), it can be observed that gearing A yields an average flow in pocket no.7 of approximately ≈ 14% across the different speeds, whereas configuration B reaches about ≈ 22%. For both cases, the flow in the central pocket is ≈ 25%.

It is now possible to address the last two questions: the effect of a different upstream pressure at the nozzle and of a different oil temperature. From a practical perspective, a change in supply pressure results in

a different flow rate. Similarly, an increase in oil temperature modifies the lubricant properties, most notably by reducing its viscosity. If the pressure is kept constant, a lower viscosity results in a higher volumetric flow rate.

Fig. 18 shows some examples of results. We can observe that, as discussed above, the general positioning of the pockets is unchanged. However, there are cases, such as the Fig. 18-(d) one, in which significant variations occur; variations that are nevertheless compensated for by the adjacent pockets. In the case of Fig. 18-(d), in fact, pocket 4 varies from 29% to 41%, while pocket 4, the adjacent one, varies from 24% to 11%. Consequently, the macroscopic oil flows do not change significantly, while variation might occur, but only on a local level.

7. Conclusions

Within the context of evaluating the oil flows inside a jet-lubricated gearboxes, this article presents to the scientific community a quantitative experimental dataset. Starting from the analysis of the literature, a new concept of test bench was defined to measure a quantity that makes it possible to understand the oil flow distribution within the system: the amount of oil collected inside pockets arranged radially with respect to the meshing zone. The rationale behind this choice, as well as the design details of the test bench, are reported in detail.

The test rig proposed here is intended and will be used for the development and validation of CFD models, currently under development. In the meantime, the test rig was designed and used prior to the development of such models in order to identify which variables influence, both qualitatively and above all quantitatively, the oil flows inside a jet-lubricated housing. An experimental campaign was therefore conducted.

The experimental result presented here consists of 96 different test conditions, in which parameters such as gear geometry, position of the active nozzles, rotational speed and its direction, and operating conditions (nozzle pressure upstream and oil temperature) were varied. The quantitative results are complemented by high-frequency recordings, some of which are also shared in video format.

Subsequently, the results are discussed to highlight the factors that have the greatest influence on the global behaviour of oil flows observed within the experimental housing. The results show that oil distribution is governed primarily by the rotation direction and by the in-mesh or out-of-mesh condition of the active nozzle, whereas rotational speed, pressure, and temperature mainly produce gradual local variations without altering the overall trends. In addition, the double-jet distributions can be reproduced by superposition of the corresponding single-jet results Although these observations refer to the specific case investigated here, the present study provides a first quantitative assessment of the mechanisms of behind oil-flow behaviour. Further analyses on different geometries and lubrication layouts will help extend these findings.

Data availability

All data are include in the article

Declaration of competing interest

The authors declare that they have no known competing financial interests or personal relationships that could have appeared to influence the work reported in this paper.

CRediT authorship contribution statement

Luca Bonaiti: Writing – review & editing, Writing – original draft, Methodology, Investigation, Data curation, Conceptualization; **Lorenzo Valsecchi:** Writing – review & editing, Writing – original draft, Visualization, Investigation; **Paolo Pisani:** Writing – review & editing, Writing – original draft, Methodology, Conceptualization; **Lorenzo Maccioni:** Writing – review & editing, Writing – original draft, Conceptualization; **Franco Concli:** Methodology, Conceptualization; **Javier Sanchez-Espiga:** Writing – review & editing, Writing – original draft, Visualization; **Carlo Gorla:** Writing – review & editing, Writing – original draft, Project administration, Methodology, Investigation, Conceptualization; **Sergio Sartori:** Writing – review & editing, Writing – original draft, Visualization, Supervision, Project administration.

Acronym

CW	ClockWise
CCW	Counter ClockWise
EASA	European Union Aviation Safety Agency
MAE	Mean Absolute Error
MGB	Main GearBox
CFD	Computational Fluid Dynamics
LDA	Laser Doppler Anemometry
PIV	Particle Image Velocimetry
SPH	Smoothed Particle Hydrodynamics

Supplementary material

Supplementary material associated with this article can be found in the online version at 10.1016/j.rineng.2026.110908.

Appendix A. Additional tests

Table A.1 enlist the results of the tests performed on gearing "A" with different nozzle pressure while Tables A.1,A.2 reports tests performed on gearing "A" with different 90 °C oil temperature. All the results averaged over the two repetition.

Table A.1
Experimental result with different oil pressure (in bar). Oil temperature is 60 °C.

Rotation		Nozzle pressure		Pockets						
Speed	Dir.	Up.	Lo.	1	2	3	4	5	6	7
500	CW	3	0	6.9	7.6	20.6	20.6	26.0	9.9	8.4
500	CW	0	3	6.5	8.3	11.3	33.3	17.9	14.3	8.3
500	CW	3	3	7.1	7.1	16.7	21.1	25.2	11.9	10.9
500	CW	5	0	6.4	7.0	16.4	23.4	21.6	14.0	11.1
500	CW	0	5	3.8	10.4	13.7	35.4	16.5	12.7	7.5
500	CW	5	5	6.3	8.9	16.5	24.1	19.9	11.5	12.6
500	CCW	3	0	0.0	15.0	13.5	43.6	17.3	9.0	1.5
500	CCW	0	3	0.0	9.8	29.3	19.5	23.2	15.9	2.4
500	CCW	3	3	1.3	8.0	24.4	29.1	24.4	11.0	1.7
500	CCW	5	0	2.3	14.5	15.0	42.8	13.9	9.2	2.3
500	CCW	0	5	1.9	10.2	29.2	18.1	21.3	16.7	2.8
500	CCW	5	5	1.1	8.4	25.9	27.2	22.2	13.7	1.6
3000	CW	3	0	11.9	6.0	10.4	29.1	23.1	6.0	13.4
3000	CW	0	3	13.1	16.7	6.0	26.2	7.1	15.5	15.5
3000	CW	3	3	11.6	9.2	8.9	32.1	17.1	8.5	12.6
3000	CW	5	0	10.4	8.1	10.4	38.2	12.1	6.9	13.9
3000	CW	0	5	11.2	15.9	6.5	27.1	7.5	16.8	15.0
3000	CW	5	5	10.1	10.6	9.0	39.2	10.3	10.1	10.8
3000	CCW	3	0	4.4	11.1	25.9	40.7	8.9	5.9	3.0
3000	CCW	0	3	2.4	6.0	22.6	29.8	31.0	6.0	2.4
3000	CCW	3	3	2.1	6.3	24.0	37.3	24.0	4.9	1.4
3000	CCW	5	0	4.6	13.9	22.0	42.2	8.1	6.9	2.3
3000	CCW	0	5	1.9	5.6	22.4	33.6	29.0	5.6	1.9
3000	CCW	5	5	2.1	7.2	22.6	39.1	21.7	5.8	1.6

Table A.2
Experimental result with 90 °C oil temperature. Oil pressure is 4 bar.

Rotation		Active nozzle		Pockets						
Speed	Dir.	Up.	Lo.	1	2	3	4	5	6	7
500	CW	0	✓	5.7	7.8	11.4	33.2	19.7	13.5	8.8
500	CW	✓	0	6.3	8.8	15.1	25.2	18.9	14.5	11.3
500	CW	✓	✓	7.5	8.1	14.4	24.8	21.3	11.0	13.0
500	CCW	0	✓	2.0	10.2	26.9	21.3	24.4	13.2	2.0
500	CCW	✓	0	2.5	13.6	16.0	39.5	16.0	9.9	2.5
500	CCW	✓	✓	1.1	7.5	25.9	27.6	24.7	12.1	1.1
3000	CW	0	✓	12.1	14.1	7.1	28.3	8.1	15.2	15.2
3000	CW	✓	0	9.9	7.5	13.0	41.0	11.2	6.2	11.2
3000	CW	✓	✓	9.2	9.2	8.6	44.3	9.8	9.2	9.8
3000	CCW	0	✓	2.0	6.0	18.6	40.2	25.1	6.0	2.0
3000	CCW	✓	0	3.8	13.8	19.5	44.0	8.8	7.5	2.5
3000	CCW	✓	✓	2.3	7.4	20.5	44.2	18.2	5.7	1.7

Appendix B. High speed recordings

Figs. B.1–B.12

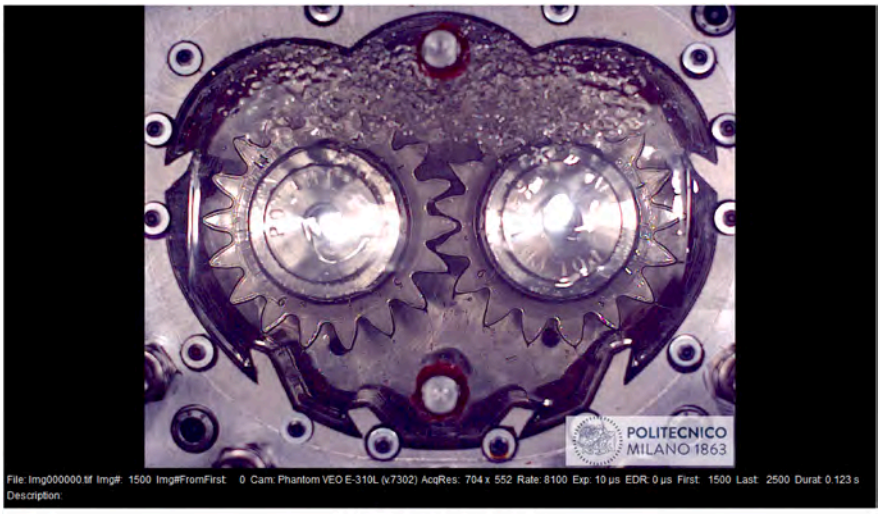

(a) *Only upper nozzle*

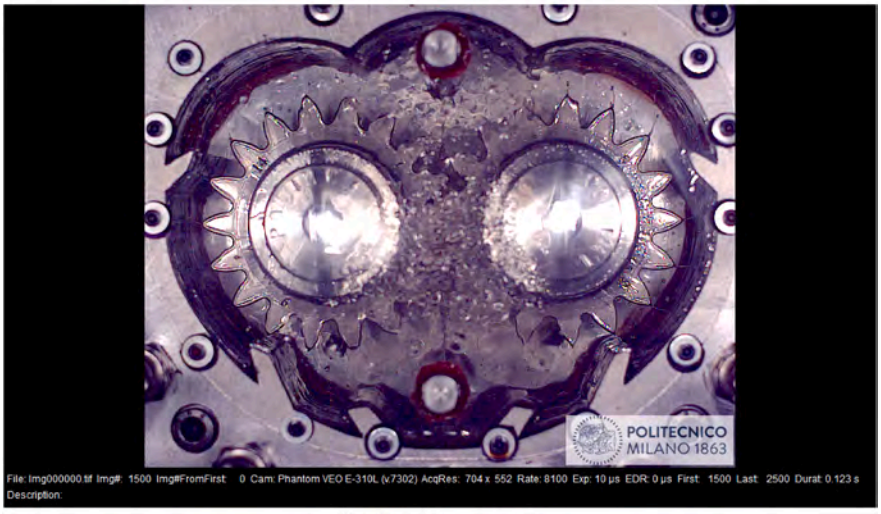

(b) *Only lower nozzle*

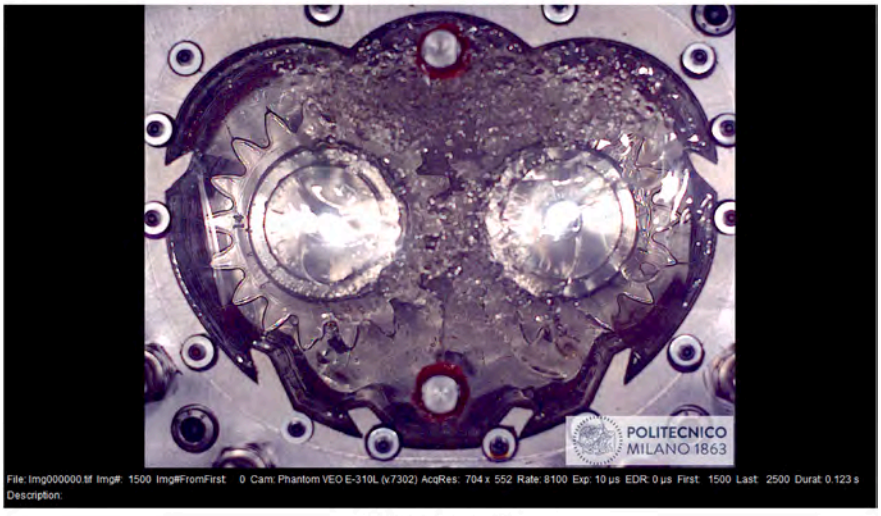

(c) *Both nozzles*

Fig. B.1. 500 rpm, CW.

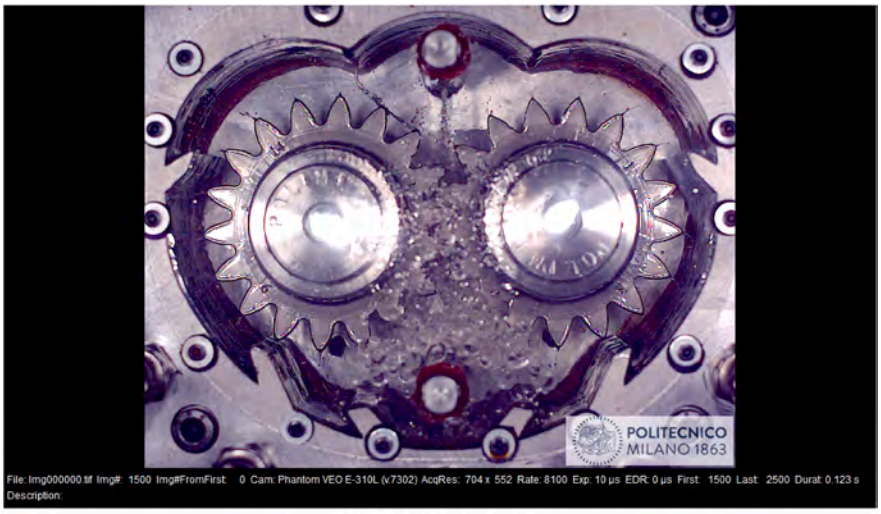

(a) *Only upper nozzle*

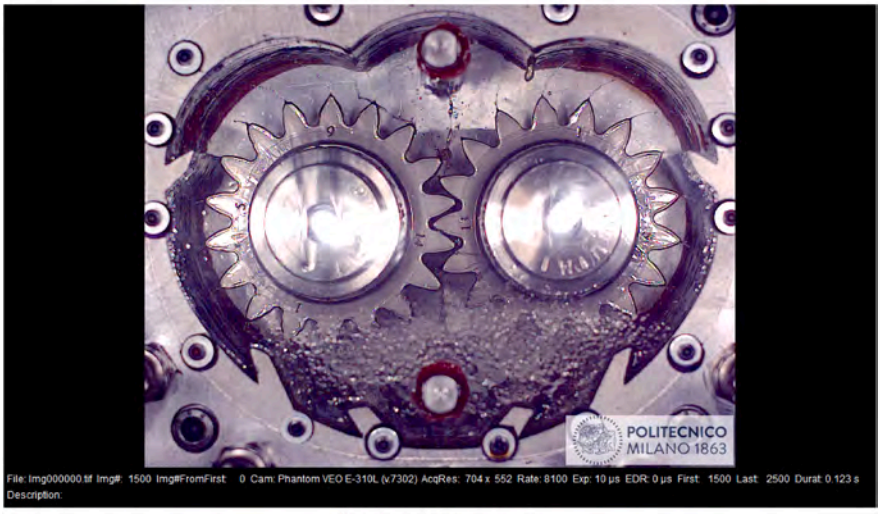

(b) *Only lower nozzle*

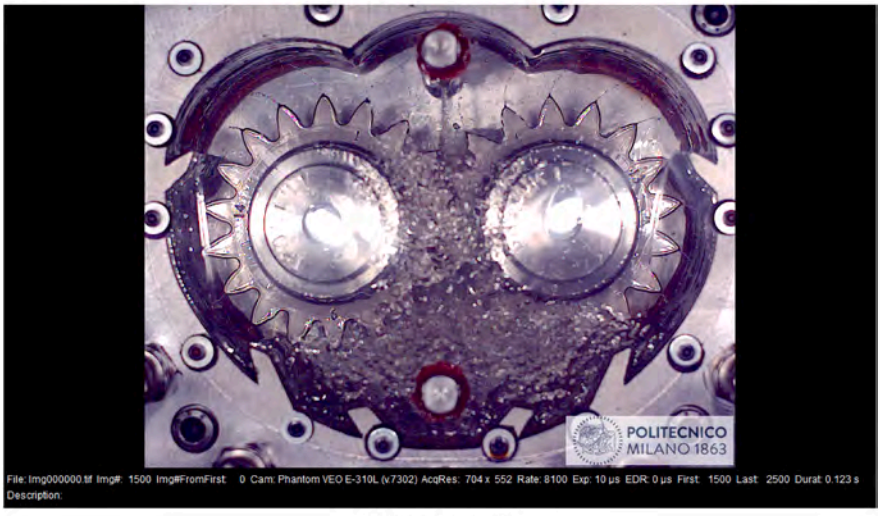

(c) *Both nozzles*

Fig. B.2. 500 rpm, CCW.

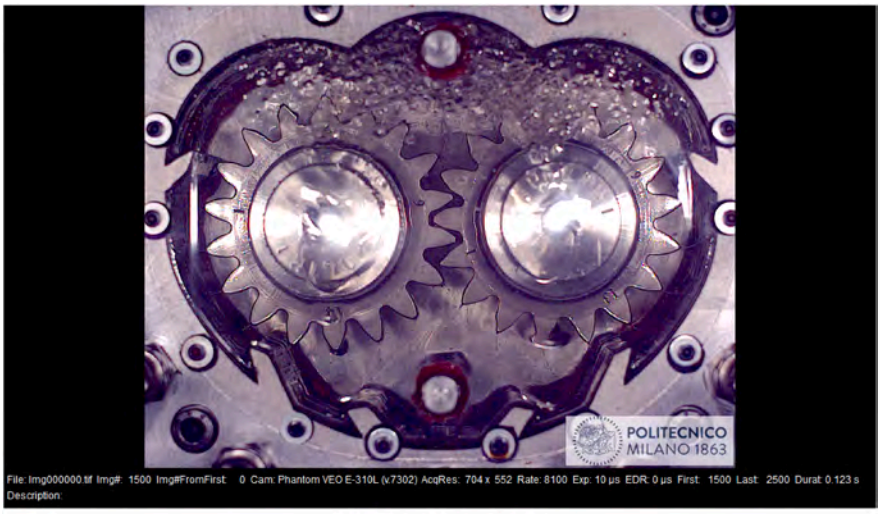

(a) *Only upper nozzle*

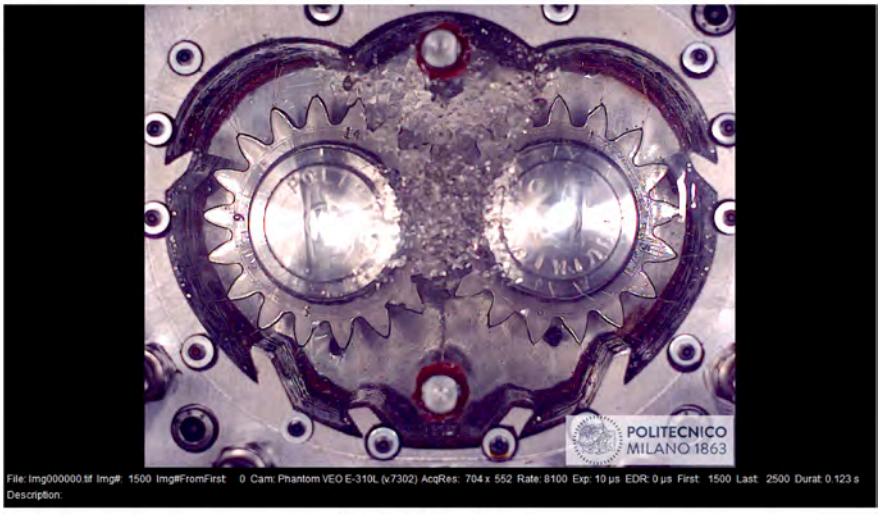

(b) *Only lower nozzle*

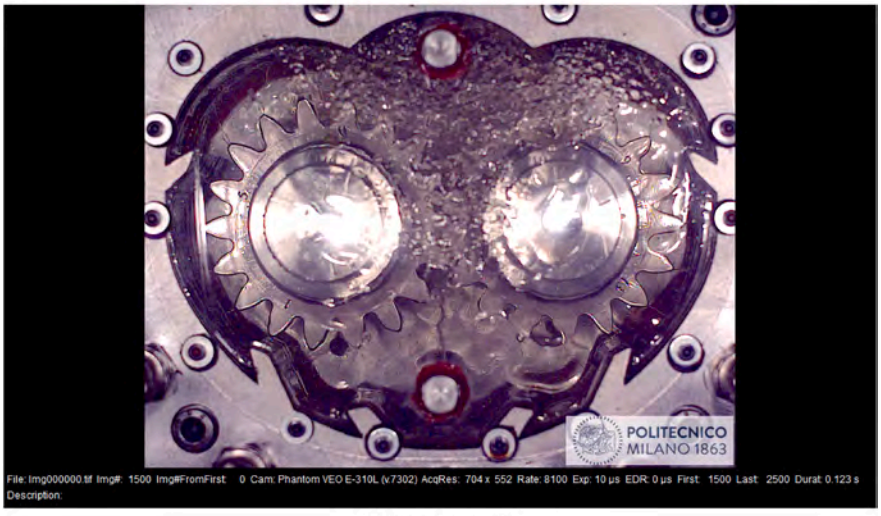

(c) *Both nozzles*

Fig. B.3. 1000 rpm, CW.

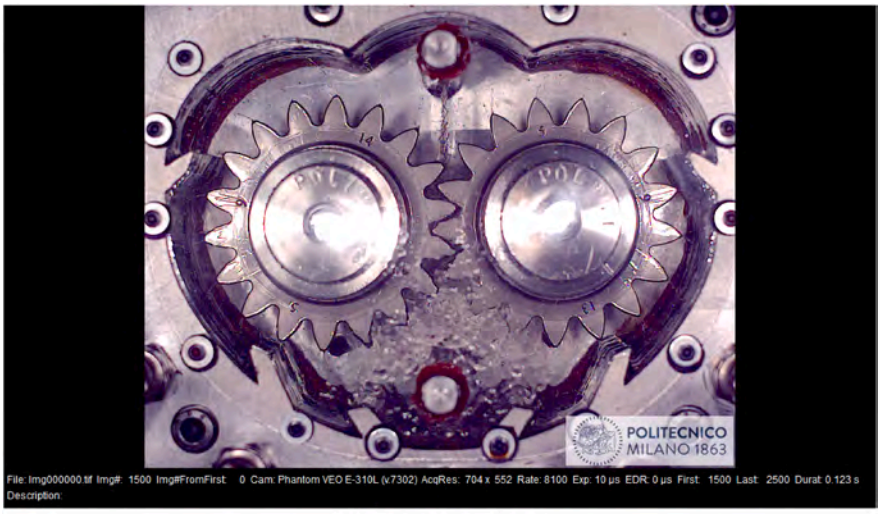

(a) *Only upper nozzle*

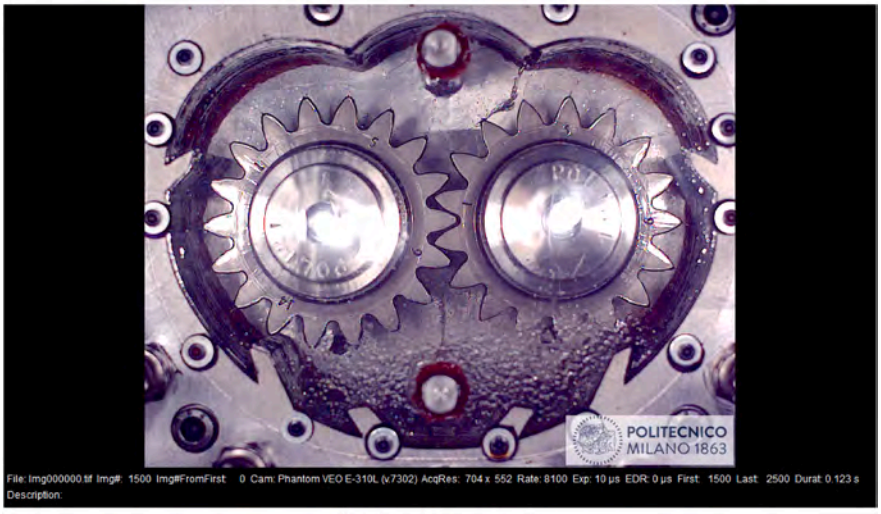

(b) *Only lower nozzle*

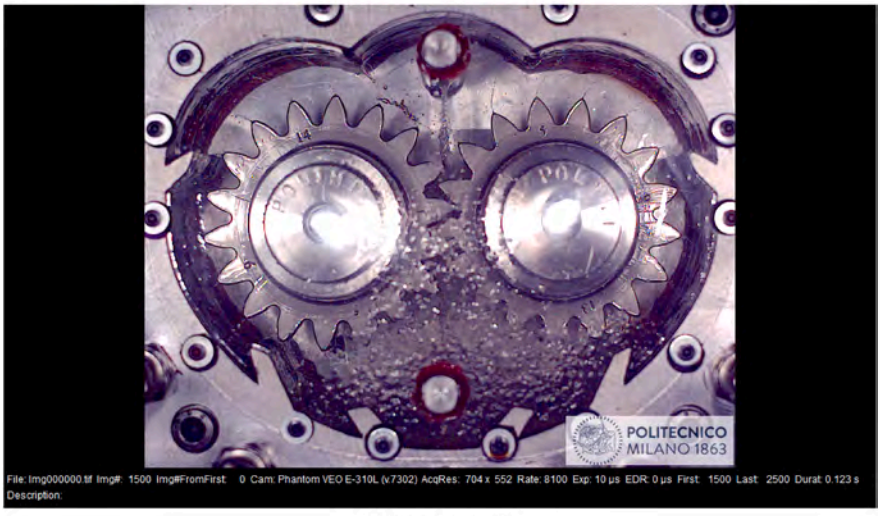

(c) *Both nozzles*

Fig. B.4. 1000 rpm, CCW.

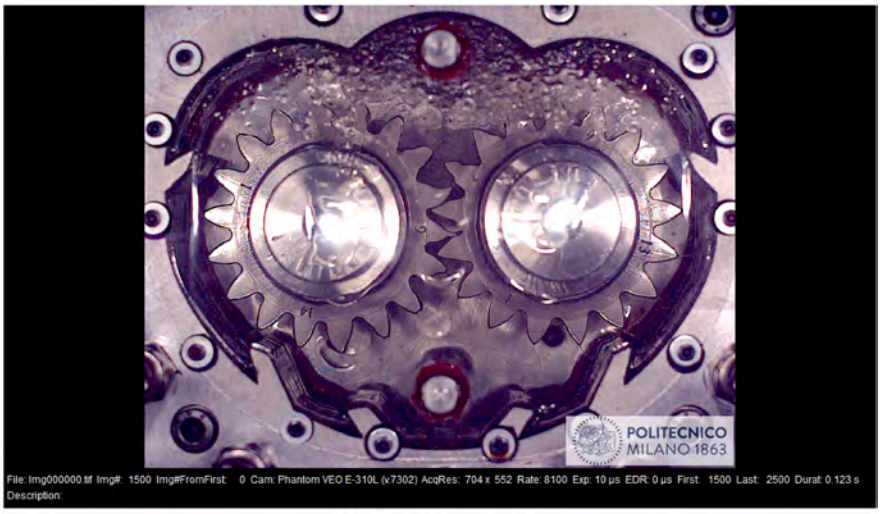

(a) *Only upper nozzle*

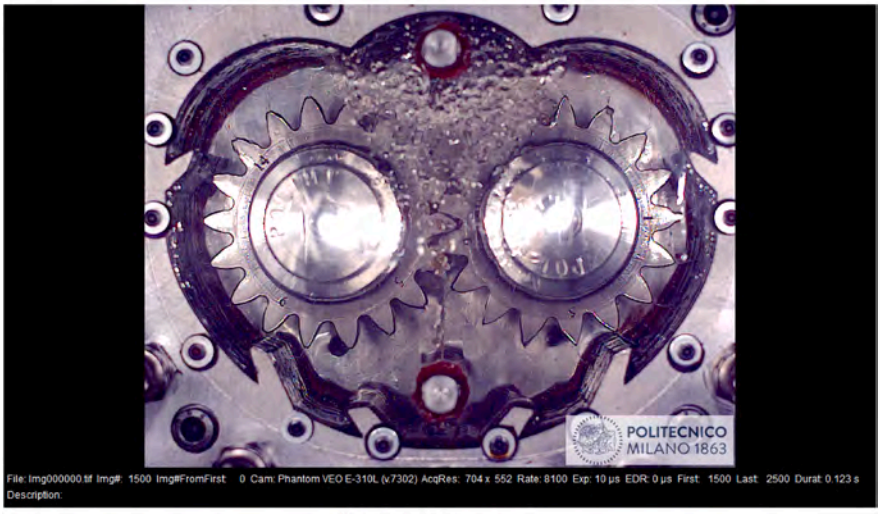

(b) *Only lower nozzle*

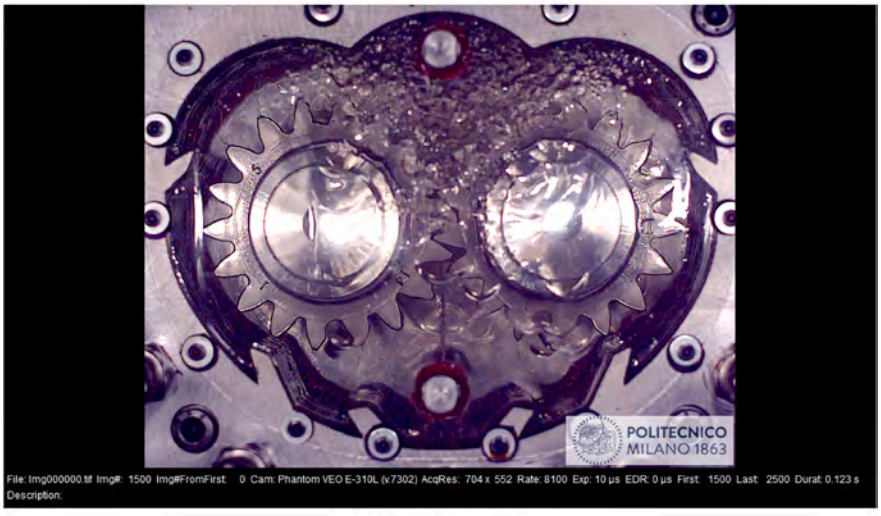

(c) *Both nozzles*

Fig. B.5. 1500 rpm, CW.

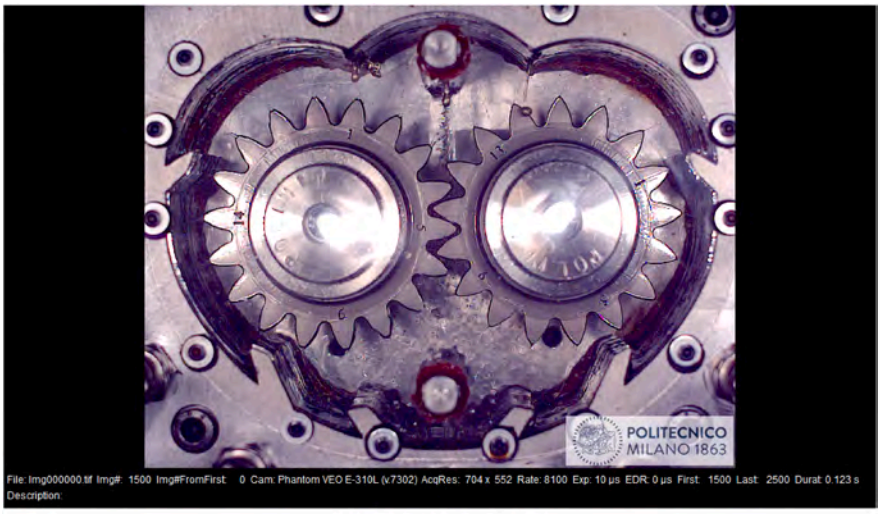

(a) *Only upper nozzle*

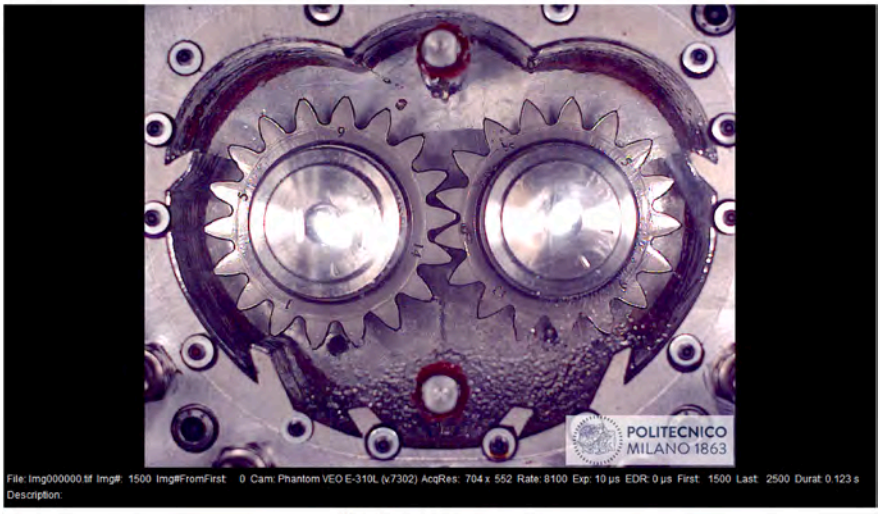

(b) *Only lower nozzle*

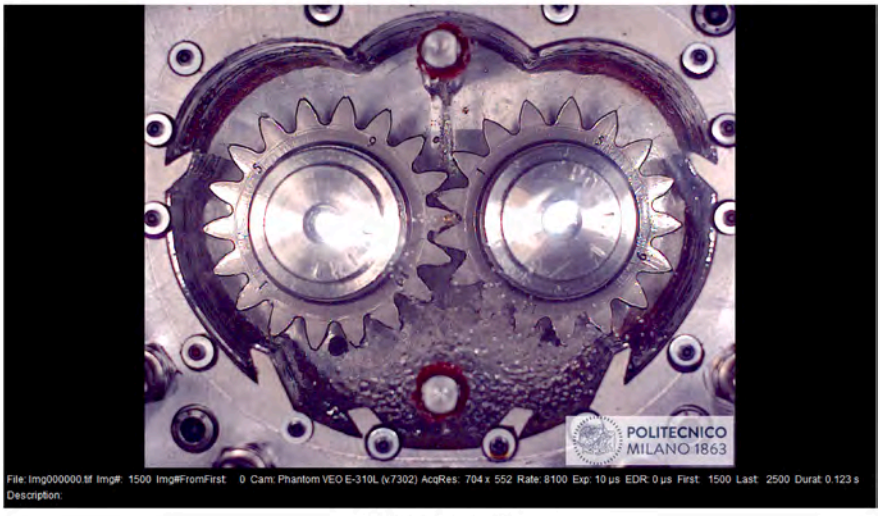

(c) *Both nozzles*

Fig. B.6. 1500 rpm, CCW.

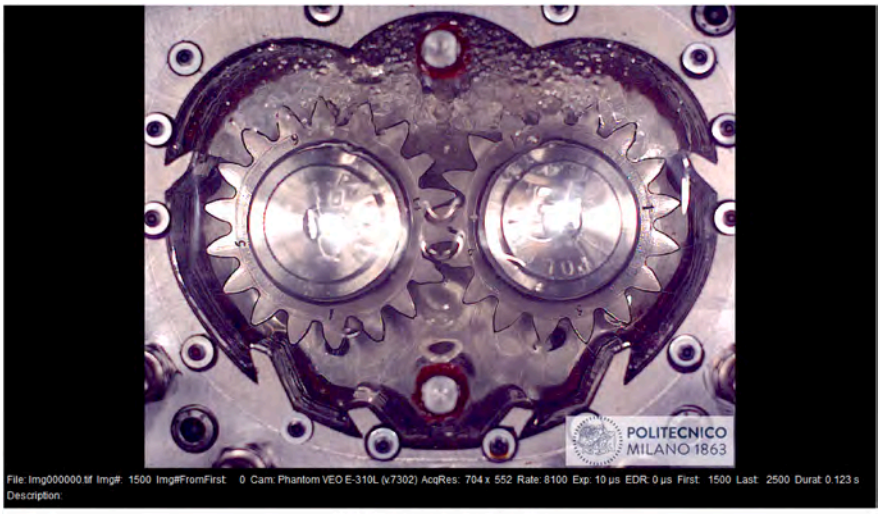

(a) *Only upper nozzle*

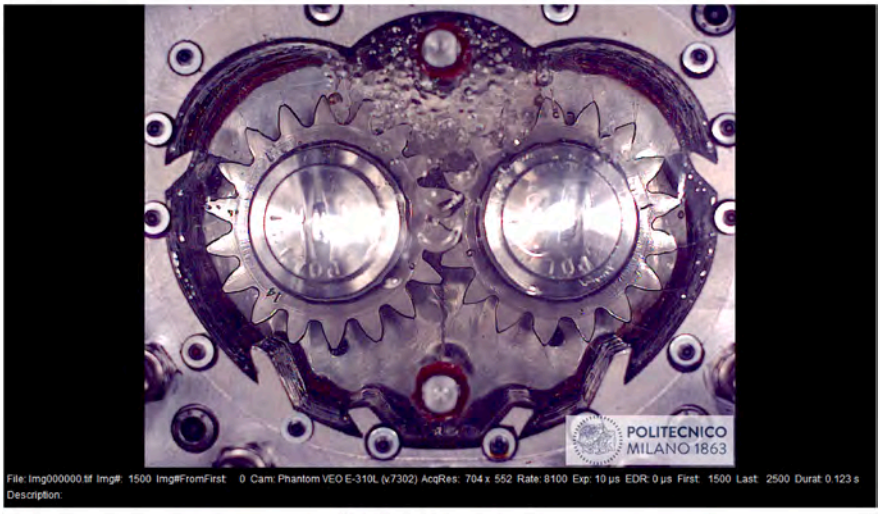

(b) *Only lower nozzle*

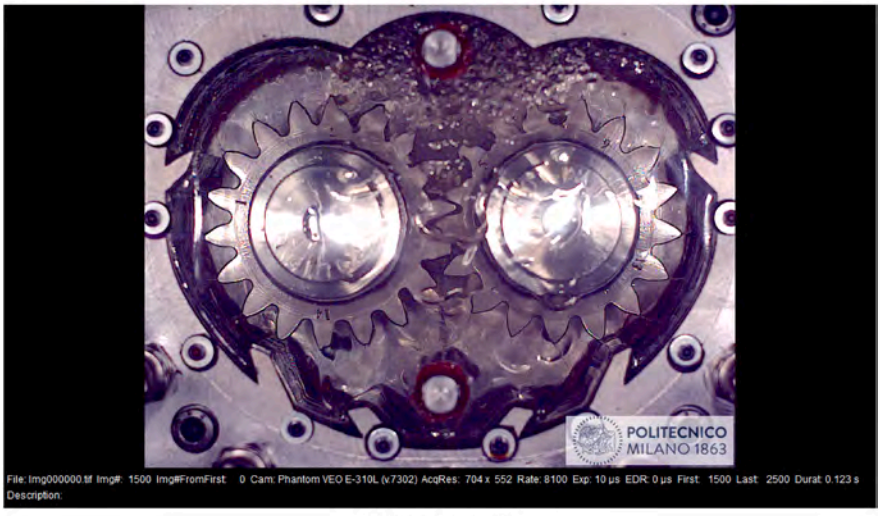

(c) *Both nozzles*

Fig. B.7. 2000 rpm, CW.

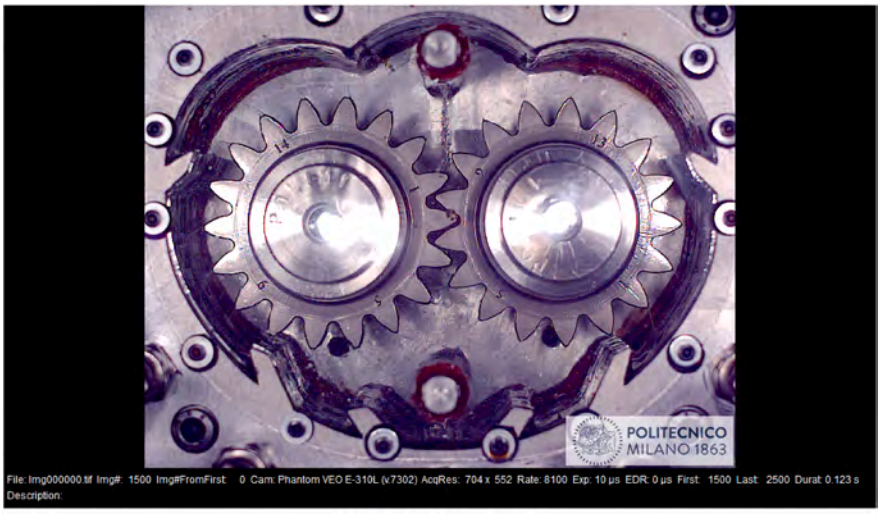

(a) *Only upper nozzle*

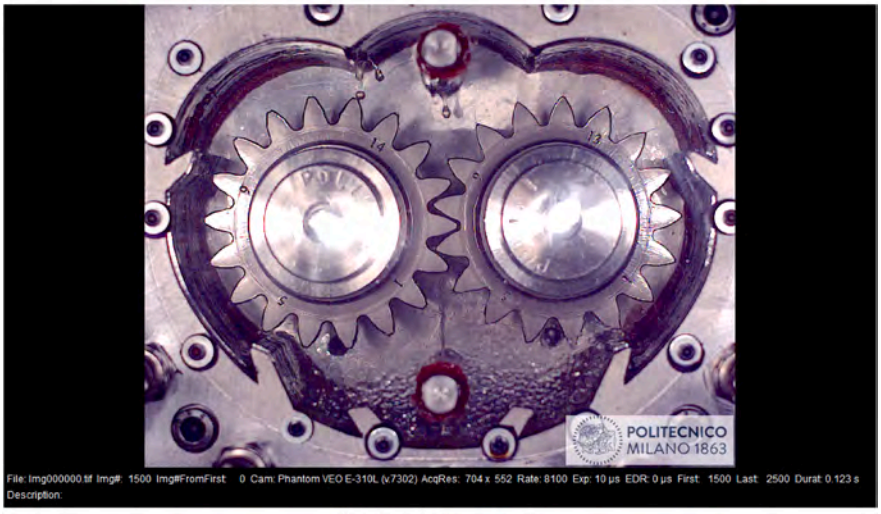

(b) *Only lower nozzle*

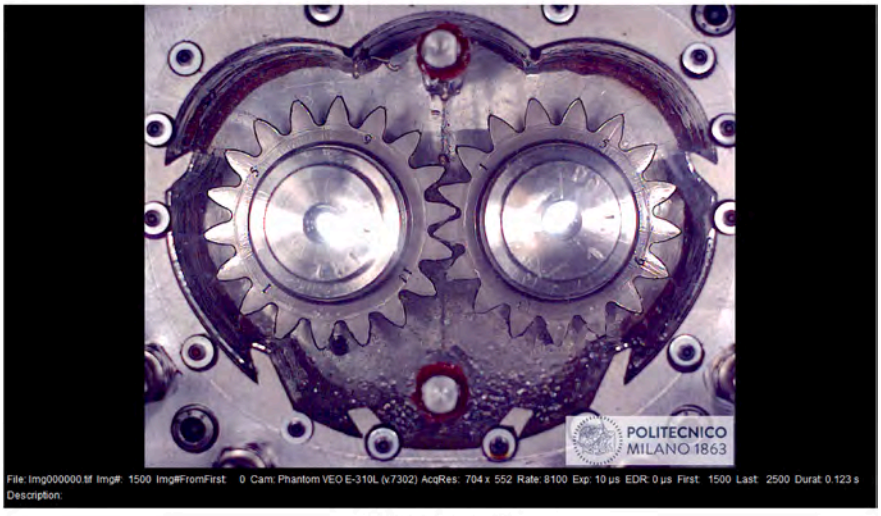

(c) *Both nozzles*

Fig. B.8. 2000 rpm, CCW.

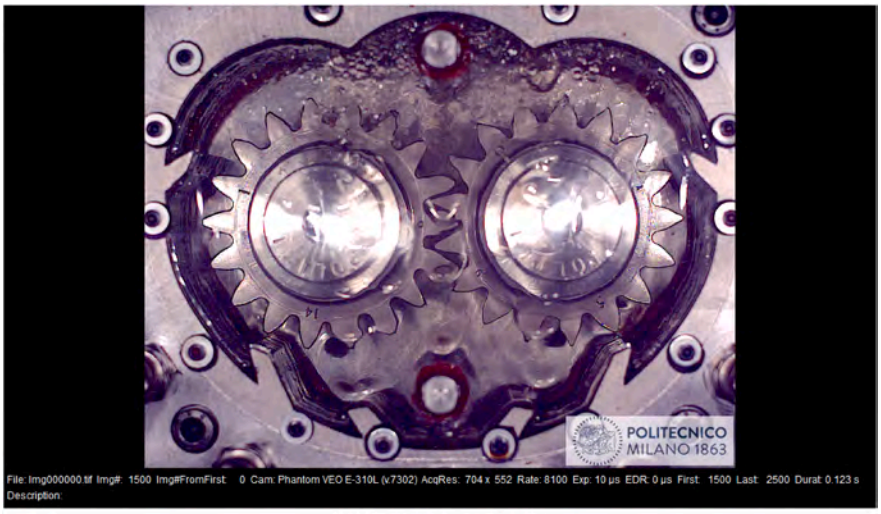

(a) *Only upper nozzle*

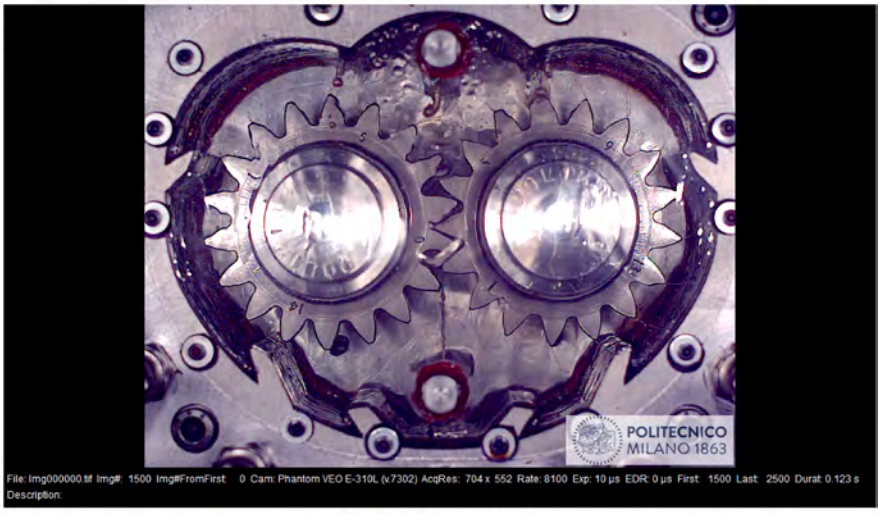

(b) *Only lower nozzle*

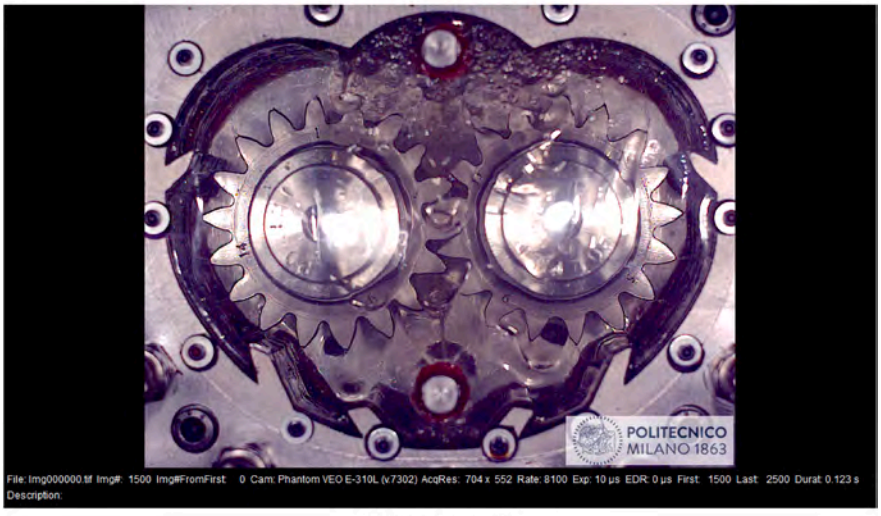

(c) *Both nozzles*

Fig. B.9. 2500 rpm, CW.

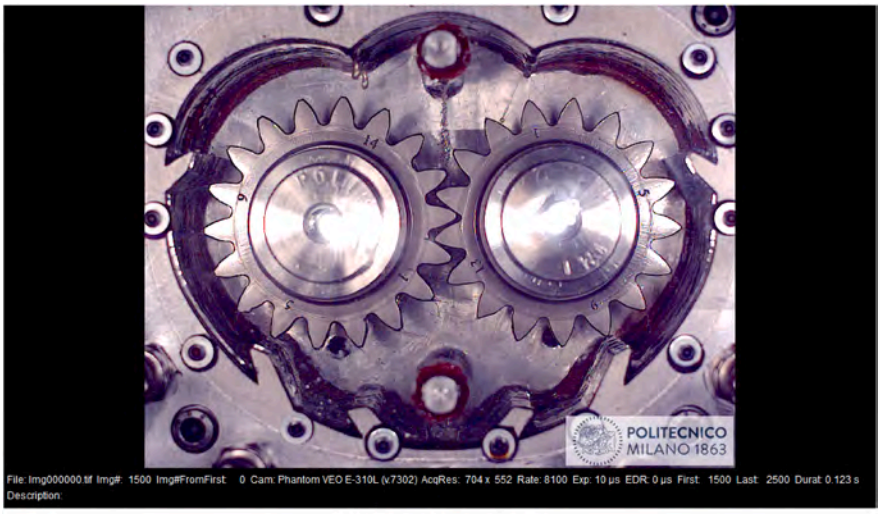

(a) *Only upper nozzle*

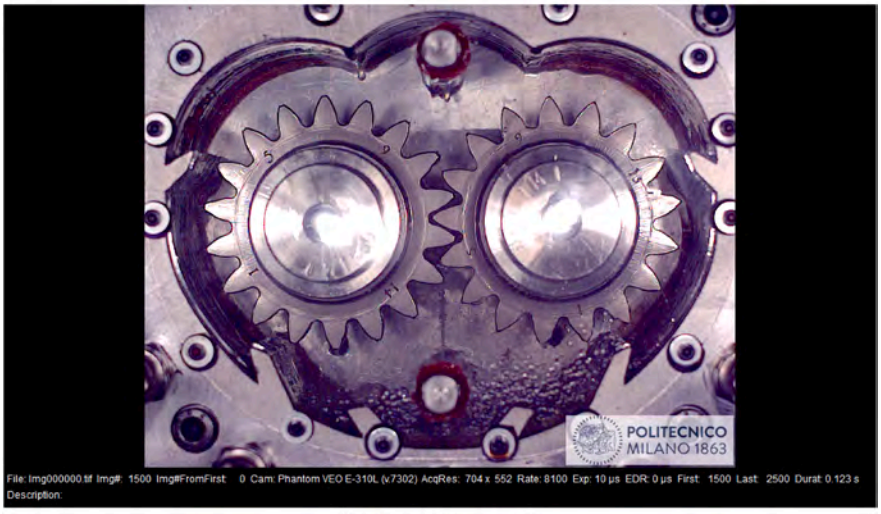

(b) *Only lower nozzle*

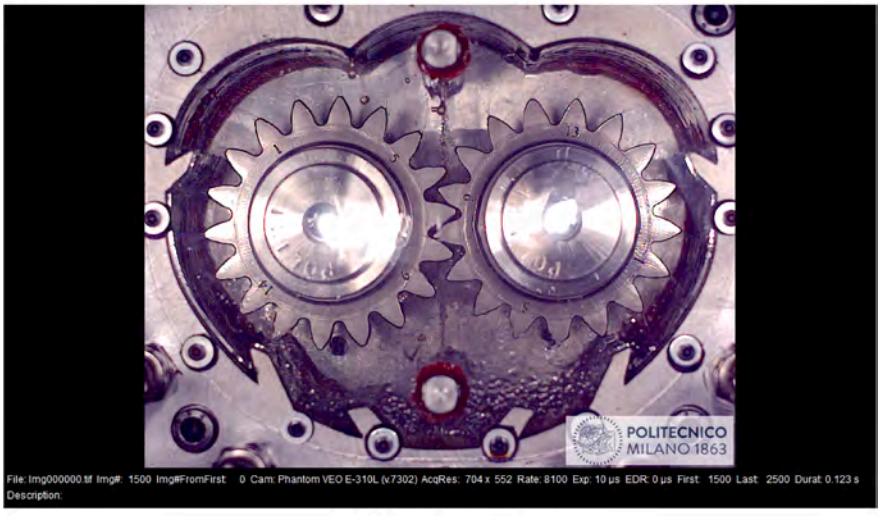

(c) *Both nozzles*

Fig. B.10. 2500 rpm, CCW.

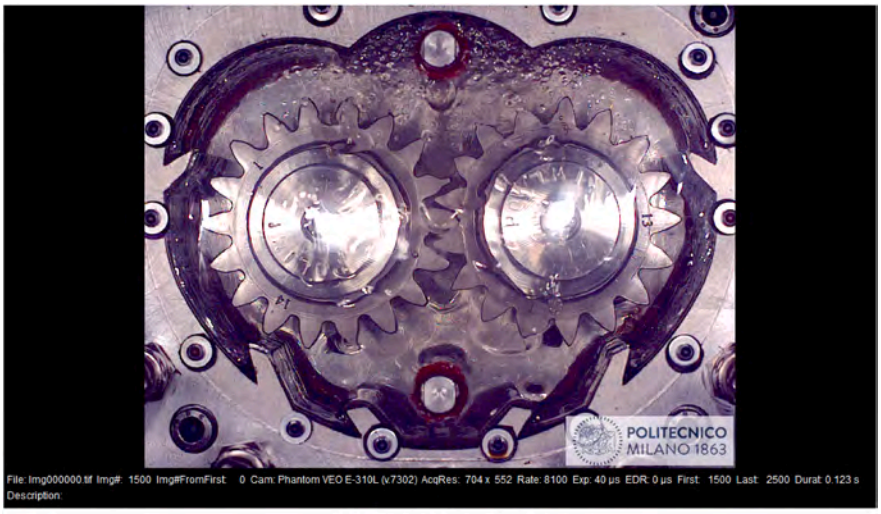

(a) *Only upper nozzle*

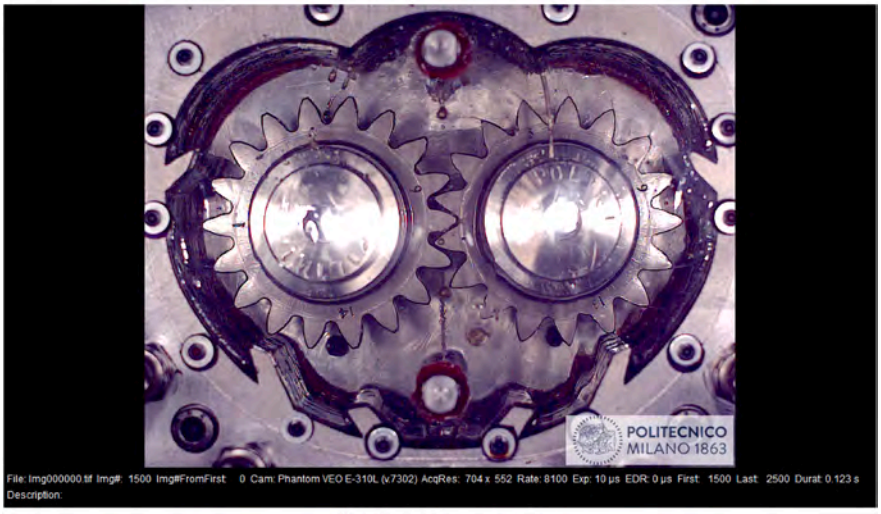

(b) *Only lower nozzle*

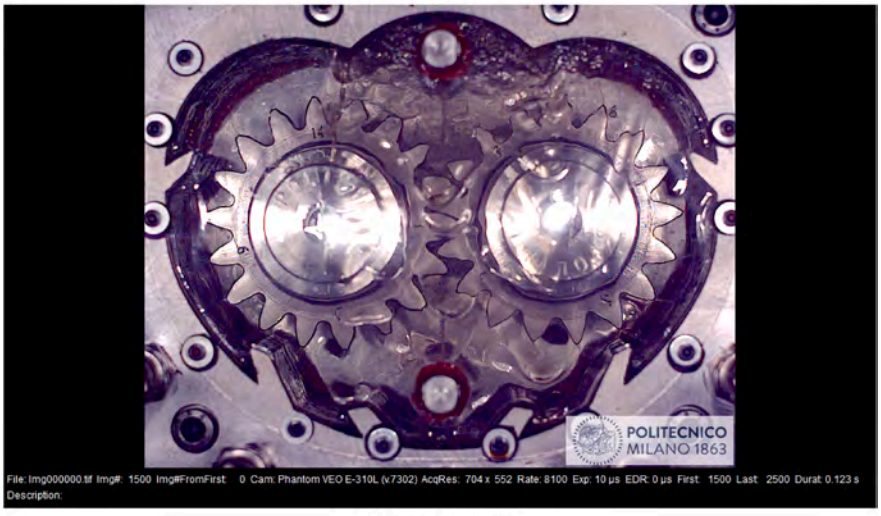

(c) *Both nozzles*

Fig. B.11. 3000 rpm, CW.

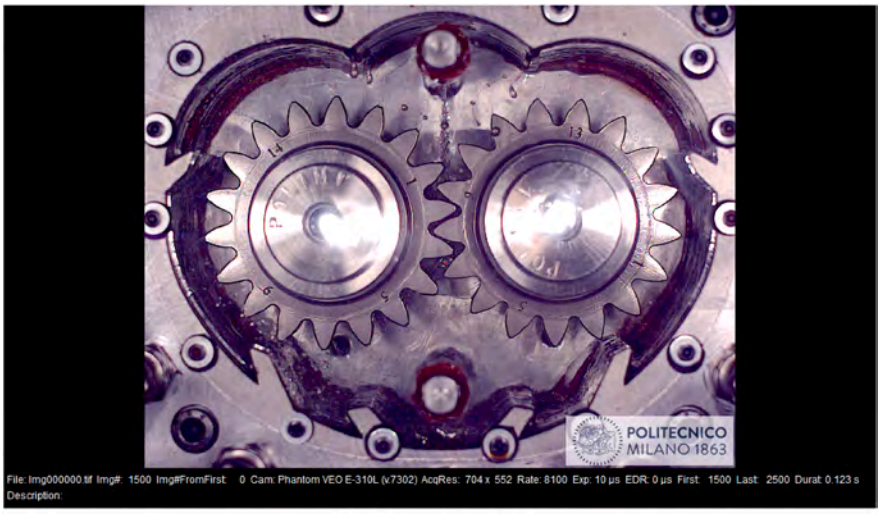

(a) *Only upper nozzle*

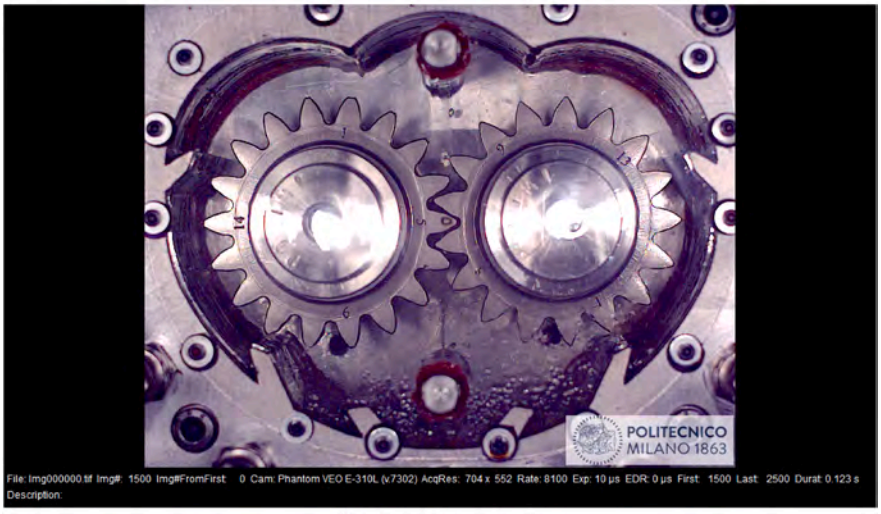

(b) *Only lower nozzle*

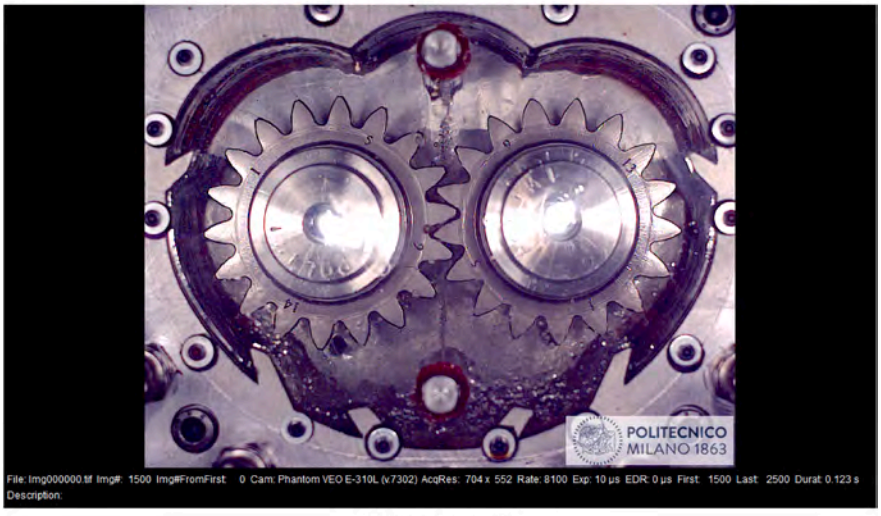

(c) *Both nozzles*

Fig. B.12. 3000 rpm, CCW.

References

[1] G. Niemann, H. Winter, B.-R. Höhn, K. Stahl, Maschinenelemente 1: Konstruktion und Berechnung von Verbindungen, Lagern, Wellen, Springer Berlin Heidelberg, Berlin, Heidelberg, Berlin, Heidelberg, 2019. https://doi.org/10.1007/978-3-662-55482

[2] EASA, Executive Director Decision 2021/016/R of 15 December 2021, Technical Report, European Union Aviation Safety Agency, 2021.

[3] EASA, EASA TYPE-CERTIFICATE DATA SHEET No. EASA.R.510 for AW189 - Issue: 12, Technical Report, European Union Aviation Safety Agency, 2025.

[4] G. Gasparini, N. Motta, A. Gabrielli, D. Colombo, Gearbox loss of lubrication performance: myth, art or science?, 40th Eur. Rotorcr. Forum 2014 2 (2014) 1162–1175.

[5] Analysis of the oil squeezing power losses of a spur gear pair by mean of CFD simulations, vol. Volume 2: in: Applied Fluid Mechanics; Electromechanical Systems and Mechatronics; Advanced Energy Systems; Thermal Engineering; Human Factors and Cognitive Engineering, Engineering Systems Design and Analysis, 2012. https://doi.org/10.1115/ESDA2012-82591

[6] F. Concli, C. Gorla, Numerical modeling of the power losses in geared transmissions: windage, churning and cavitation simulations with a new integrated approach that drastically reduces the computational effort, Tribol. Int. 103 (2016) 58–68. https://doi.org/10.1016/j.triboint.2016.06.046

[7] F. Concli, C. Gorla, CFD simulation of power losses and lubricant flows in gearboxes, Am. Gear Manuf. Assoc. Fall Tech. Meet. 2017 2017 (2017) 2–14.

[8] M.N. Mastrone, F. Concli, CFD simulations of gearboxes: implementation of a mesh clustering algorithm for efficient simulations of complex system's architectures, Int. J. Mech. Mater. Eng. 16 (1) (2021). https://doi.org/10.1186/s40712-021-00134-6

[9] M.N. Mastrone, F. Concli, CFD simulation of grease lubrication: analysis of the power losses and lubricant flows inside a back-to-back test rig gearbox, J. Non-Newton. Fluid Mech. 297 (2021) 104652. https://doi.org/10.1016/j.jnnfm.2021.104652

[10] L. Maccioni, F. Concli, Exploring the potential of CFD in gear jet lubrication design: a systematic literature review, Forsch. Ingenieurwes. 89 (1) (2025) 1–19.

[11] L.S. Akin, J.J. Mross, D.P. Townsend, Study of lubricant jet flow phenomena in spur gears, J. Lubr. Technol. 97 (2) (1975) 283–288. https://doi.org/10.1115/1.3452576

[12] D.P. Townsend, L.S. Akin, Study of lubricant jet flow phenomena in spur gears-out of mesh condition, J. Mech. Des. 100 (1) (1978) 61–68. https://doi.org/10.1115/1.3453894

[13] L.S. Akin, D.P. Townsend, Into mesh lubrication of spur gears with arbitrary offset oil jet. part 1: for jet velocity less than or equal to gear velocity, J. Mech. Transm. Autom. Des. 105 (4) (1983) 713–718. https://doi.org/10.1115/1.3258541

[14] L.S. Akin, D.P. Townsend, Into mesh lubrication of spur gears with arbitrary offset oil jet. part 2: for jet velocities equal to or greater than gear velocity, J. Mech. Transm. Autom. Des. 105 (4) (1983) 719–724. https://doi.org/10.1115/1.3258542

[15] L.S. Akin, J.J. Mross, Theory for the effect of windage on the lubricant flow in the tooth spaces of spur gears, J. Eng. Ind. 97 (4) (1975) 1266–1272. https://doi.org/10.1115/1.3438742

[16] D.P. Townsend, L.S. Akin, Gear lubrication and cooling experiment and analysis, NASA Conf. Publ. 1 (1983) 470–490.

[17] Y. Ariura, T. UENO, T. Sunaga, S. Sunamoto, The lubricant churning loss in spur gear systems, Bull. JSME 16 (95) (1973) 881–892. https://doi.org/10.1299/jsme1958.16.881

[18] H. Mizutani, Y. Isikawa, D.P. Townsend, Effects of lubrication on the performance of high speed spur gears, NASA Conf. Publ. 1 (1989) 327–334.

[19] V. Chernoray, M. Jahanmiri, Experimental study of multiphase flow in a model gearbox, in: Computational Methods in Multiphase Flow VI, 70, 2011, p. 153–164. https://doi.org/10.2495/MPF110131

[20] R.F. Handschuh, M.J. Hurrell, Initial experiments of high-speed drive system windage losses, NASA Technical Note TM 2011 216925 (2011) 1–17.

[21] R.F. Handschuh, M.J. Hurrell, Initial experiments of high-speed drive system windage losses, Int. Conf. Gears 1 (2011) 1–17.

[22] E.A. Hartono, M. Golubev, V. Chernoray, PIV study of fluid flow inside a gearbox, in: PIV13; 10th International Symposium on Particle Image Velocimetry, Delft, The Netherlands, July 1–3, 2013, Delft University of Technology, 2013, pp. 1–11.

[23] H. Arisawa, M. Nishimura, H. Imai, T. Goi, Wang201influenceofspin, J. Eng. Gas Turbines Power 136 (9) (2014) 092604. https://doi.org/10.1115/1.4026952

[24] Y. Wang, W. Niu, S. Wei, G. Song, Influence of spin flow on lubricating oil jet-design method of oil spray parameters to high speed spur gears, Tribol. Int. 92 (2015) 290–300. https://doi.org/10.1016/j.triboint.2015.07.017

[25] P.M.T. Marques, C.M.C.G. Fernandes, R.C. Martins, J.H.O. Seabra, Efficiency of a gearbox lubricated with wind turbine gear oils, Tribol. Int. 71 (2014) 7–16. https://doi.org/10.1016/j.triboint.2013.10.017

[26] E.A. Hartono, A. Pavlenko, V. Chernoray, Stereo-PIV study of oil flow inside a model gearbox, in: 17th International Symposium on Applications of Laser Techniques to Fluid Mechanics, 2014, pp. 07–10.

[27] Velocity measurements in the vicinity of the exit and inlet of a spiral bevel gear shroud, vol. Volume 5C: Heat Transfer Turbo Expo, 2015. https://doi.org/10.1115/GT2015-43549

[28] P.M.T. Marques, R. Camacho, R.C. Martins, J.H.O. Seabra, Efficiency of a planetary multiplier gearbox: influence of operating conditions and gear oil formulation, Tribol. Int. 92 (2015) 272–280. https://doi.org/10.1016/j.triboint.2015.06.018

[29] C.M.C.G. Fernandes, R.C. Martins, J.H.O. Seabra, Torque loss of type C40 FZG gears lubricated with wind turbine gear oils, Tribol. Int. 70 (2014) 83–93. https://doi.org/10.1016/j.triboint.2013.10.003

[30] C.M.C.G. Fernandes, P.M.T. Marques, R.C. Martins, J.H.O. Seabra, Gearbox power loss. Part II: friction losses in gears, Tribol. Int. 88 (2015) 309–316. https://doi.org/10.1016/j.triboint.2014.12.004

[31] C.M.C.G. Fernandes, L. Blazquez, J. Sanesteban, R.C. Martins, J.H.O. Seabra, Energy efficiency tests in a full scale wind turbine gearbox, Tribol. Int. 101 (2016) 375–382. https://doi.org/10.1016/j.triboint.2016.05.001

[32] F. Concli, Thermal and efficiency characterization of a low-backlash planetary gearbox: an integrated numerical-analytical prediction model and its experimental validation, Proc. Inst. Mech. Eng. J: J. Eng. Tribol. 230 (8) (2016) 996–1005. https://doi.org/10.1177/1350650115622363

[33] S.-W. Chen, S. Matsumoto, Influence of relative position of gears and casing wall shape of gear box on churning loss under splash lubrication condition-some new ideas, Tribol. Trans. 59 (6) (2016) 993–1004. https://doi.org/10.1080/10402004.2015.1129568

[34] D. Massini, T. Fondelli, B. Facchini, L. Tarchi, F. Leonardi, High speed visualizations of oil jet lubrication for aero-engine gearboxes, Upstream Connect Error or Disconnect/reset before Headers. Reset Reason: Connection Termination 101 (2016) 1248–1255. ATI 2016 - 71st Conference of the Italian Thermal Machines Engineering Association. j.egypro.2016.11.140

[35] Y. Wang, G. Song, Study on calculation method of gear temperature field based on spray lubrication, SAE Tech. Pap. 2017 (2017). https://doi.org/10.4271/2017-01-2444

[36] Y. Wang, G. Song, W. Niu, Y. Chen, Optimized design of spray parameters of oil jet lubricated spur gears, Tribol. Int. 120 (2018) 149–158. j.triboint.2017.12.042

[37] I.R. Delgado, M.J. Hurrell, Baseline experimental results on the effect of oil temperature on shrouded meshed spur gear windage power loss Volume 10: 2017 ASME International Power Transmission and Gearing Conference (2017) V010T11A040. https://doi.org/10.1115/DETC2017-67818

[38] I. Delgado, M. Hurrell, Experimental investigation of shrouding on meshed spur gear windage power loss, Annu. Forum Proc. - AHS Int. 1 (2017) 2267–2275.

[39] J.-B. Boni, A. Neurouth, C. Changenet, F. Ville, Experimental investigations on churning power losses generated in a planetary gear set, J. Adv. Mech. Des. Syst. Manuf. 11 (6) (2017) JAMDSM0079. https://doi.org/10.1299/jamdsm.2017jamdsm0079

[40] S. Miladinović, S. Radosavljević, S. Veličković, R. Atyat, A. Skulić, V. Šljivić, Optimization of efficiency of worm gear reducer by using taguchi-grey method, Appl. Eng. Lett. 2 (2) (2017) 69–75.

[41] A. Skulić, B. Stojanović, S. Radosavljević, S. Veličković, Experimental determination of worm gearing efficiency, Appl. Eng. Lett. 4 (4) (2019) 115–119. https://doi.org/10.18485/aeletters.2019.4.4.2

[42] D. Massini, T. Fondelli, A. Andreini, B. Facchini, L. Tarchi, F. Leonardi, Experimental and numerical investigation on windage power losses in high speed gears, Proc. ASME Turbo Expo 2017: Turbomach. Tech. Conf. Expo. Volume 5B: Heat Transfer (2017) V05BT15A034. https://doi.org/10.1115/GT2017-64948

[43] D. Massini, T. Fondelli, A. Andreini, B. Facchini, L. Tarchi, F. Leonardi, Experimental and numerical investigation on windage power losses in high speed gears, J. Eng. Gas Turbines Power 140 (8) (2018) 082508. https://doi.org/10.1115/1.4038471

[44] H. Liu, T. Jurkschat, T. Lohner, K. Stahl, Determination of oil distribution and churning power loss of gearboxes by finite volume CFD method, Tribol. Int. 109 (2017) 346–354. j.triboint.2016.12.042

[45] S. Laruelle, C. Fossier, C. Changenet, F. Ville, S. Koechlin, Experimental investigations and analysis on churning losses of splash lubricated spiral bevel gears, Mech. Ind. 18 (4) (2017) 412. https://doi.org/10.1051/meca/2017007

[46] A. Neurouth, C. Changenet, F. Ville, M. Octrue, E. Tinguy, Experimental investigations to use splash lubrication for high-speed gears, J. Tribol. 139 (6) (2017) 061104. https://doi.org/10.1115/1.4036447

[47] ASME (Ed.), Classification of fluid dynamic loss in aeroengine transmission gears: experimental analysis and CFD validation, vol. Volume 1: Aircraft Engine; Fans and Blowers; Marine; Honors and Awards Turbo Expo, 2017. https://doi.org/10.1115/GT2017-63208

[48] J. Moss, A. Kahraman, C. Wink, An experimental study of influence of lubrication methods on efficiency and contact fatigue life of spur gears, J. Tribol. 140 (5) (2018) 051103. https://doi.org/10.1115/1.4039929

[49] J. Polly, D. Talbot, A. Kahraman, A. Singh, H. Xu, An experimental investigation of churning power losses of a gearbox, J. Tribol. 140 (3) (2018) 031102. https://doi.org/10.1115/1.4038412

[50] H. Liu, G. Arfaoui, M. Stanic, L. Montigny, T. Jurkschat, T. Lohner, K. Stahl, Numerical modelling of oil distribution and churning gear power losses of gearboxes by smoothed particle hydrodynamics, Proc. Inst. Mech. Eng. J J. Eng. Tribol. 233 (1) (2019) 74–86. https://doi.org/10.1177/1350650118760626

[51] R. Quiban, C. Changenet, Y. Marchesse, F. Ville, J. Belmonte, Churning losses of spiral bevel gears at high rotational speed, Proc. Inst. Mech. Eng. J J. Eng. Tribol. 234 (2) (2020) 172–182. https://doi.org/10.1177/1350650119858236

[52] Y. Dai, J. Jia, B. Ouyang, J. Bian, Determination of an optimal oil jet nozzle layout for helical gear lubrication: mathematical modeling, numerical simulation, and experimental validation, Complexity 2020 (1) (2020) 2187027. https://doi.org/10.1155/2020/2187027

[53] M.N. Mastrone, E.A. Hartono, V. Chernoray, F. Concli, Oil distribution and churning losses of gearboxes: experimental and numerical analysis, Tribol. Int. 151 (2020) 106496. https://doi.org/10.1016/j.triboint.2020.106496

[54] A. Dindar, K. Chaudhury, I. Hong, A. Kahraman, C. Wink, An experimental methodology to determine components of power losses of a gearbox, J. Tribol. 143 (11) (2021) 111203. https://doi.org/10.1115/1.4049940

[55] B. Zhu, X. Wang, L. Luo, N. Zhang, X. Liu, Influence of lubricant supply on thermal and efficient performances of a gear reducer for electric vehicles, J. Tribol. 144 (1) (2021) 011202. https://doi.org/10.1115/1.4052681

[56] H.G. Chothani, K.D. Maniya, Comparative investigation of worm positions for worm gear-box performance under no-load condition, J. Mech. Eng. 18 (2) (2021) 111–124. https://doi.org/10.24191/JMECHE.V18I2.14967

[57] H.G. Chothani, K.D. Maniya, Experimental investigation on churning power loss of splash lubricated worm gear, Period. Polytech. Mech. Eng. 67 (3) (2023) 175–182. https://doi.org/10.3311/PPme.19965
[58] L. Hildebrand, F. Dangl, M. Sedlmair, T. Lohner, K. Stahl, CFD analysis on the oil flow of a gear stage with guide plate; [CFD-Analyse der Ölströmung in einem Getriebe mit Leitblech], Forsch. Ingenieurwes./Eng. Res. 86 (3) (2022) 395–408. https://doi.org/10.1007/s10010-021-00523-5
[59] B. Legrady, M. Taesch, G. Tschirschnitz, C.F. Mieth, Prediction of churning losses in an industrial gear box with spiral bevel gears using the smoothed particle hydrodynamic method; [Simulation der Planschverluste in einem spiralverzahnten Industriekegelradgetriebe mithilfe der Smoothed Particle Hydrodynamics Methode], Forsch. Ingenieurwes./Eng. Res. 86 (3) (2022) 379–388. https://doi.org/10.1007/s10010-021-00514-6
[60] M. Andersson, M. Sosa, U. Olofsson, Efficiency and temperature of spray lubricated superfinished spur gears, Proc. Inst. Mech. Eng. J J. Eng. Tribol. 236 (11) (2022) 2283–2291. https://doi.org/10.1177/13506501221077773
[61] J.F. Shore, A.S. Kolekar, N. Ren, A. Kadiric, An investigation into the influence of viscosity on gear churning losses by considering the effective immersion depth, Tribol. Trans. 66 (5) (2023) 906–919. https://doi.org/10.1080/10402004.2023.2247041
[62] X. Zhu, Y. Dai, Development of an analytical model to predict the churning power losses of an orthogonal face gear, Eng. Sci. Technol. Int. J. 41 (2023) 101383. https://doi.org/10.1016/j.jestch.2023.101383
[63] L. Li, S. Wang, Experimental study and numerical analysis on windage power loss characteristics of aviation spiral bevel gear with oil injection lubrication, Stroj. Vestn./J. Mech. Eng. 69 (5-6) (2023) 235–247. https://doi.org/10.5545/sv-jme.2023.558
[64] D. Guo, G. Wen, Y. Wang, D. Luo, A theoretical and experimental study on the power loss of gearbox based on dimensionless analysis, J. Tribol. 145 (10) (2023) 101701. https://doi.org/10.1115/1.4062449
[65] M. Handschuh, A. Guner, A. Kahraman, An experimental investigation of windage and oil churning power losses of gears and discs, Proc. Inst. Mech. Eng. J J. Eng. Tribol. 237 (1) (2023) 163–177. https://doi.org/10.1177/13506501221104372
[66] Z. Qingyong, F. Zhen, J. Mingjun, C. Shanyou, Analysis and verification of splash lubrication for electric vehicle gearbox, Int. J. Heavy Veh. Syst. 29 (6) (2023) 627–646. https://doi.org/10.1504/IJHVS.2022.129788
[67] W. Ramdane, C. Changenet, S. Seghir Ouali, C. Chevrel-Fraux, P. Casanova, Thermal model of a planetary gear set using an isothermal approach, VDI Ber. 2023 (2422) (2023) 451–466. https://doi.org/10.51202/9783181024225-451
[68] W. Ramdane, C. Changenet, S. Seghir-Ouali, C. Chevrel-Fraux, P. Casanova, Transient thermal model of a planetary gear set based on a uniform temperature approach; [Transient thermisches Modell eines Planetengetriebes basierend auf einem einheitlichen Temperaturansatz], Forsch. Ingenieurwes./Eng. Res. 87 (3) (2023) 1117–1127. https://doi.org/10.1007/s10010-023-00710-6
[69] T. Torres, C. Changenet, T. Touret, B. Guilbert, A new experimental methodology to study convective heat transfer in oil jet lubricated gear units, Lubricants 11 (9) (2023). https://doi.org/10.3390/lubricants11090408
[70] M.N. Mastrone, L. Hildebrand, C. Paschold, T. Lohner, K. Stahl, F. Concli, Numerical and experimental analysis of the oil flow in a planetary gearbox, Appl. Sci. 13 (2) (2023). https://doi.org/10.3390/app13021014
[71] C. Kunik, J. Kunert, Wetting and oil flow analysis of planetary gearboxes using oil flow simulations, VDI Ber. 2023 (2422) (2023) 467–484. Cited by: 0. https://doi.org/10.51202/9783181024225-467
[72] M. Reichl, P. Lenz, A. Oliva, Challenges and possibilities of virtual development of e-axle transmissions: SPH-Simulation with PreonLab, VDI Ber. 2023 (2422) (2023) 485–498. https://doi.org/10.51202/9783181024225-485
[73] Y. Dai, X. Chen, D. Yang, X. Zhu, Impulse power loss in orthogonal face gear-numerical and experimental results, Eur. Phys. J. Plus 138 (1) (2023). Cited by: 8. https://doi.org/10.1140/epjp/s13360-023-03653-7
[74] X. Jiang, C. Zhou, J. Su, G. Jin, R. Shen, Injection parameter design to improve the high-speed gear heat dissipation: CFD simulation and regression orthogonal experiment, Simul. Model. Pract. Theory 128 (2023) 102795. https://doi.org/10.1016/j.simpat.2023.102795
[75] K. Suzuki, K. Sakai, K. Sakai, T. Hara, Considerations on lubrication of high-speed rotating gear (first report): relationship between the lubricating oil behavior and airflow on the tooth surface, VDI Ber. 2023 (2422) (2023) 741–752. https://doi.org/10.51202/9783181024225-741
[76] D.J. Marsonia, N.N. Jadeja, S.H. Zala, N.D. Mehta, H.G. Chothani, H.G. Vyas, Experimental investigation of nitrided helical gear with different helix angles for oil drag power loss, SSRG Int. J. Mech. Eng. 11 (6) (2024) 105–114. https://doi.org/10.14445/23488360/IJME-V11I6P112
[77] L. Hildebrand, P. Beierer, T. Lohner, K. Stahl, Numerical calculation of the oil flow in a truck rear axle transmission and the influence of gear-induced air flow, J. Tribol. 146 (11) (2024) 114602. https://doi.org/10.1115/1.4065872
[78] H.G. Chothani, K.S. Vaghosi, D.J. Marsonia, N.N. Jadeja, S.H. Zala, Influence of lubricant type on churning power loss of worm gear, Tribol. Mater. 3 (4) (2024) 178–186. https://doi.org/10.46793/tribomat.2024.019
[79] S. Yan, Z. Kong, H. Liu, L. Zhang, X. Hu, Y. Hou, Power loss evaluation of an E-axle gearbox considering the influence of gear oil factors, Lubricants 12 (1) (2024). https://doi.org/10.3390/lubricants12010011
[80] Z. Qiao, C. Zhou, J. Su, X. Jiang, A novel dynamic heat-flow coupled model under spray lubrication for high-speed gears: CFD simulation and experimental validation, Simul. Model. Pract. Theory 131 (2024) 102867. j.simpat.2023.102867
[81] X. Hu, Y. Yuan, J. Chen, Study on temperature field distribution of a high-speed double-helical gear pair with oil injection lubrication, Lubricants 12 (9) (2024). https://doi.org/10.3390/lubricants12090315
[82] E. Tomanik, N. Getschko, G. Papoulias, B. Lemos, J. Silva, Development of a gearbox test rig to evaluate the impact of oil formulations on churning and friction losses, Proc. Inst. Mech. Eng. J J. Eng. Tribol. 239 (6) (2025) 751–766. https://doi.org/10.1177/13506501241301833
[83] M. Reichl, P. Lenz, Virtual optimization of gearbox oiling–How reliable are the results, in: International Conference on Gears 2025, VDI Wissensforum, VDI Wissensforum, Duesseldorf, Germany, 2025, pp. 105–114.
[84] B. Cardozo, R. Rego, R. Metzger da Silva, Quantitative analysis of churning in dip-lubricated gearboxes through computer vision techniques, in: International Conference on Gears 2025, VDI Wissensforum, VDI Wissensforum, Duesseldorf, Germany, 2025, pp. 189–203.
[85] M. Ohno, K. Suzuki, T. Hara, K. Sakai, K. Sakai, J. Yamada, Consideration on lubrication of high-speed rotating gear (second report), in: International Conference on Gears 2025, VDI Wissensforum, VDI Wissensforum, Duesseldorf, Germany, 2025, pp. 275–282.
[86] C. C. Kunik, C. Nau, T. Goldschmidt, Simulative evaluation of heat transfer and surface temperature distribution of an industrial gear unit, in: International Conference on Gears 2025, VDI Wissensforum, VDI Wissensforum, Duesseldorf, Germany, 2025, pp. 369–388.
[87] P. Neuenfeldt, J. Dorffer, A. Steurer, P. Leoni, Approach to determine quantitatively correct load- independent power losses inside turbo gearboxes by flow simulation - Combined meshless and mesh-based flow simulations, in: International Conference on Gears 2025, VDI Wissensforum, VDI Wissensforum, Duesseldorf, Germany, 2025, pp. 543–552.
[88] M. Cardaun, M. Gebhardt, Improving the efficiency of a wind turbine gearbox with modern CFD methods, in: International Conference on Gears 2025, VDI Wissensforum, VDI Wissensforum, Duesseldorf, Germany, 2025, pp. 643–654.
[89] X. Chu, Y. Liu, Z. Shang, Study on oil film spreading characteristics on the jet lubricating tooth surface of aviation herringbone gear, Ind. Lubr. Tribol. 77 (6) (2025) 1045–1059. https://doi.org/10.1108/ILT-08-2023-0250
[90] J. Seabra, K. Michaelis, B. Höhn, M. Hinterstoißer, Influence factors on gearbox power loss, Ind. Lubr. Tribol. 63 (1) (2011) 46–55. https://doi.org/10.1108/00368791111101830
[91] A. Mihailidis, I. Nerantzis, A new system for testing gears under variable torque and speed, Recent Pat. Mech. Eng. 2 (3) (2009) 179–192. https://doi.org/10.2174/2212797610902030179
[92] T.T. Petry-Johnson, A. Kahraman, N.E. Anderson, D.R. Chase, An experimental investigation of spur gear efficiency, J. Mech. Des. 130 (6) (2008) 062601. https://doi.org/10.1115/1.2898876
[93] G. Niemann, H. Winter, Maschinenelemente Band 2: Getriebe allgemein, Zahnradgetriebe - Grundlagen, Stirnradgetriebe, Springer Berlin Heidelberg, 2003. https://doi.org/10.1007/978-3-662-11873-3
[94] P.V. Ceresa, Experimental Analysis of the Oil Flows in a Single-Stage Jet-Lubricated Spur Gear Transmission, Politecnico di Milano, Scuola di Ingegneria Industriale e dell'Informazione, 2025.
[95] J.R. Colbourne, The Geometry of Involute Gears, Springer New York, New York, NY, New York, NY, 1987. https://doi.org/10.1007/978-1-4612-4764-7